Geothermics 85 (2020) 101763

Contents lists available at ScienceDirect

Geothermics

journal homepage: www.elsevier.com/locate/geothermics

# Travertine deposits constraining transfer zone neotectonics in geothermal areas: An example from the inner Northern Apennines (Bagno Vignoni-Val d'Orcia area, Italy)

Andrea Brogi[a,b,*], Domenico Liotta[a,b], Enrico Capezzuoli[c], Paola Francesca Matera[a], Sándor Kele[d], Michele Soligo[e], Paola Tuccimei[e], Giovanni Ruggieri[f], Tsai-Luen Yu[g,h], Chuan-Chou Shen[g], Katharine W. Huntington[i]

[a] University of Bari, Department of Earth and Geoenvironmental Sciences, Via Orabona 4, Bari, Italy
[b] IGG-CNR, Institute of Geosciences and Earth Resources, Via Moruzzi 1, Pisa, Italy
[c] University of Florence, Department of Earth Sciences, Via La Pira 4, Florence, Italy
[d] Institute for Geological and Geochemical Research, Research Centre for Astronomy and Earth Sciences, MTA Centre for Excellence, Budapest, Hungary
[e] University of Rome3, Department of Science, Largo San L. Murialdo 1, Roma, Italy
[f] IGG-CNR, Institute of Geosciences and Earth Resources, Via La Pira 4, Firenze, Italy
[g] High-Precision Mass Spectrometry and Environment Change Laboratory (HISPEC), Department of Geosciences, National Taiwan University, Taipei 10617, Taiwan, ROC
[h] Research Center for Future Earth, National Taiwan University, Taipei, 10617, Taiwan, ROC
[i] Department of Earth and Space Sciences, University of Washington, Seattle, WA 98195, United States

ARTICLE INFO

*Keywords:*
Travertine
Low-Temperature geothermal areas
Seismotectonic setting
Tectonic activity
Extensional tectonics

ABSTRACT

Studying travertine deposits and the network of banded calcite veins that form their roots in the substratum can place important constraints on neotectonic activity and the seismotectonic settings of geothermal areas. In this paper, we present the results of integrated studies of a geothermal area located in the inner Northern Apennines (Bagno Vignoni area, Italy), where low magnitude ($M < 4$) seismicity suggests the occurrence of active faults, but information on their location, time-span of activity and seismotectonic setting is lacking. The study area is characterised by thermal springs ($T < 50\,^{\circ}C$) and travertine deposits well exposed in saw-cut walls of abandoned quarries. We investigate the relationships between faults and the travertine deposits, in order to reconstruct the syn-sedimentary tectonic activity and the age of faulting, by combining analyses of: i) geological setting and structural/kinematic analyses of faults; ii) travertine morpho-structural and architectural setting; iii) travertine facies; iv) U-Th radiometric, stable- and clumped isotopes of travertine and banded calcite veins. The results highlight the occurrence of a wide brittle shear zone (> 3 km) formed by two orthogonal faults systems, NE- and NW-striking, characterised by oblique-slip to normal kinematics, respectively; these faults belong to a tract of the so-named "Grosseto-Pienza" transfer zone, crossing the southern Tuscany from the sea-cost to the outer Apennines belt. The Grosseto-Pienza transfer zone formed with extensional tectonics that have been affecting the inner Northern Apennines since the middle Miocene. U-Th dating of travertine and banded calcite veins indicates that faulting enhanced the hydrothermal fluid circulation since the middle Pleistocene, in an unvaried tectonic setting, as indicated by the $\delta^{18}O$ signature and temperature of the hydrothermal fluids, which remained stable through time. The activity of the faults continued until the Holocene and still produces seismicity. Finally, our findings permit to define the seismo-tectonic setting of this sector of the inner Northern Apennines, demonstrating more broadly the utility of travertine deposits in reconstructing the neotectonics in geothermal areas.

## 1. Introduction

Fault transfer zones consist of km-wide deformed crustal volumes, formed by parallel and/or anastomosed fault segments that accommodate heterogeneous extension, splitting the thinned crust into domains characterised by differentiated amount of extension (Gibbs, 1990). Transfer zones are therefore wide brittle shear zones coexisting with near orthogonal normal faults, and contributing to produce lithospheric and crustal thinning, as described for several regions affected by extensional tectonics in continental crustal environments

* Corresponding author at: University of Bari, Department of Earth and Geoenvironmental Sciences, Via Orabona 4, Bari, Italy.
*E-mail address:* andrea.brogi@uniba.it (A. Brogi).

https://doi.org/10.1016/j.geothermics.2019.101763
Received 8 April 2019; Received in revised form 27 September 2019; Accepted 8 November 2019
Available online 26 November 2019
0375-6505/ 

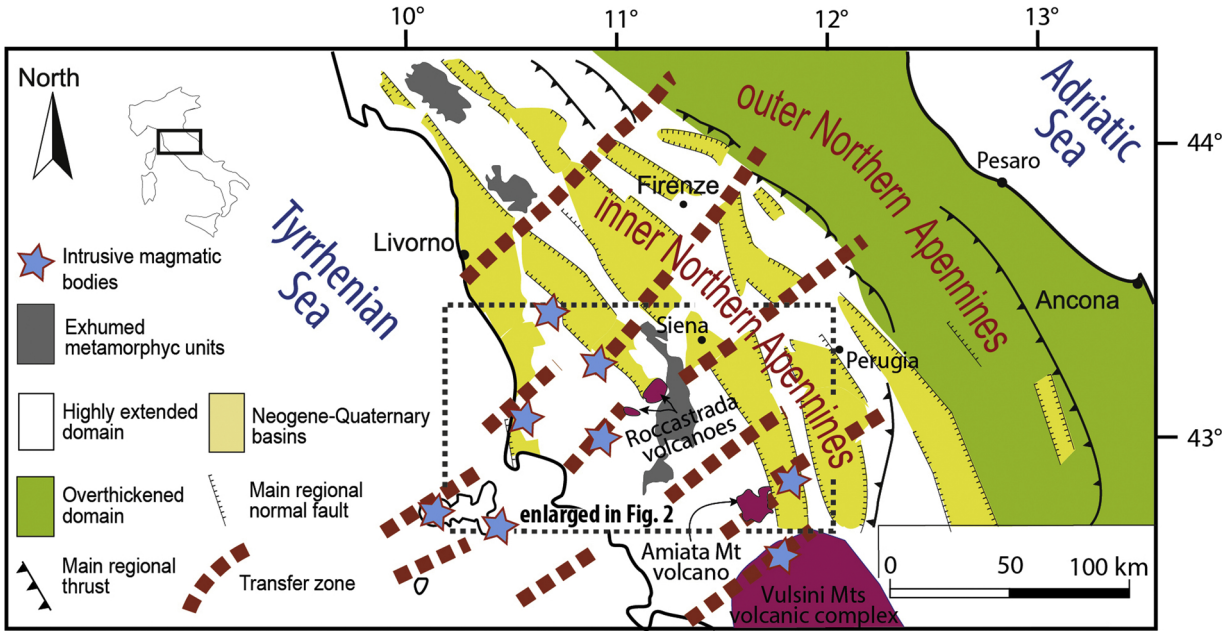


**Fig. 1.** Tectonic sketch of the inner and outer Northern Apennines showing the main structural features: exhumed HP-metamorphic units, Neogene magmatic bodies, basin-and-range structure with associated transfer zones in the inner zone; thrusts and developing basins in the outer zone.

(Bally, 1981; Gibbs, 1990). In this framework, transfer zones result as highly fractured rock-volumes where fluids can easily channelled (Lister et al., 1986; Ebinger, 1989; Gibbs, 1990; Liotta, 1991; Rowland and Sibson, 2004; Alçiçek et al., 2013; Liotta et al., 2015), thus having a role in controlling the emplacement of magmatic bodies in the upper crustal levels (Dini et al., 2008) and in favouring the circulation of geothermal fluids (e.g. Rowland and Sibson, 2004).

The coexistence of normal and transfer fault zones has been documented in the inner Northern Apennines, Italy, since at least the Neogene (Liotta, 1991; Carmignani et al., 1995; Liotta et al., 1998; Brogi et al., 2005a; Brogi and Liotta, 2008; Barchi, 2010; Liotta et al., 2015), when magmatism and related hydrothermal circulation were related to continuous (still ongoing) extensional processes, with a prominent SW-NE-oriented distribution along the main transfer zones (Fig. 1). The present configuration of the inner Northern Apennines (i.e. southern Tuscany and Northern Latium; Carmignani et al., 2001) and northern Tyrrhenian sea (Bartole, 1995; Pascucci et al., 1999) derives from a rifting process that thinned the lithosphere up to 30 – 50 km, (Calcagnile and Panza, 1981; Locardi and Nicolich, 1992) and the crust up to 20 – 26 km (Di Stefano et al., 2011 with references therein), after the final thickening process related to the Oligocene-early Miocene nappe stacking (Brunet et al., 2001; Molli, 2008; Rossetti et al., 2015).

In southern Tuscany, the NE-trending transfer zones were initially indicated as tectonic lineaments (Fig. 1) since the early 1900s, by studies describing their geometric setting, geological features and geomorphological evidences (Signorini, 1935; Merla, 1951; Ghelardoni, 1965; Bortolotti, 1966). However, detailed field-based information on their architecture and kinematics is restricted to only a few areas (Liotta, 1991; Pascucci et al., 2007; Brogi et al., 2013, 2014; Bianchi et al., 2015), where the role of the structures associated to the transfer zones in controlling Neogene-Quaternary magmatism (Dini et al., 2008; Acocella and Funiciello, 2006; Brogi et al., 2010a; Liotta et al., 2015) and seismicity (Mantovani et al., 1995; Albarello et al., 2005; Viti et al., 2006; Brogi and Fabbrini, 2009; Viti et al., 2016) has been emphasized.

In the Monte Amiata (Fig. 1) volcano-geothermal area (Brogi, 2008a; Batini et al., 2003), NE-trending faults have been considered as the main structures controlling the evolution of the middle Pleistocene volcano (Mazzuoli et al., 1995; Ferrari et al., 1996; Cadoux and Pinti, 2009; Brogi et al., 2010a) and the development of Hg-Sb ore deposits (Brogi et al., 2011). In a similar scenario, NE-trending structures were strictly associated with the Pleistocene volcanism of the Northern Latium (Acocella and Funiciello, 1999, 2006) and magmatism in the northern Tyrrhenian Sea (Dini et al., 2008; Liotta et al., 2015).

Low-magnitude seismicity associated with these structures (Buonasorte et al., 1987; Liotta, 1991; Brogi et al., 2014; Mantovani et al., 2015; Piccardi et al., 2017) suggests their tectonic activity, at least in some tracts. This topic is almost important as the seismotectonic setting of the inner Northern Apennines is poorly defined, and scarce data are available to infer active and potentially dangerous faults. A profound knowledge of NE-trending structures is needed to better constrain their potential impact on the seismicity of southern Tuscany, and their role in controlling geothermal fluids circulation and storage at depth.

We address these issues by presenting an integrated method of study that includes sedimentological, structural and geochemical analyses, focussing on the travertine deposition, as a marker of the fluid-rock interaction through time. The study area is located in the sector of the inner Northern Apennines (Val d'Orcia, Bagno Vignoni area), to the north of the Monte Amiata volcano-geothermal area (Fig. 2), where a first-order NE-trending transfer zone (Grosseto-Pienza tectonic lineament in Bemporad et al., 1986) has been documented since the 1980's (e.g., Bemporad et al., 1986), and where low-magnitude seismicity also occurs (http://cnt.rm.ingv.it/). Thermal springs and widespread travertine deposits (active and fossil) are aligned along this structure, indicating a strong relationship between faulting and fluid flow. Our study is aimed to define: i) the geometrical and kinematics settings of faults; ii) the role of these structures in channelling and controlling the fluid-rock interaction of the hydrothermal fluids flow through time; iii) the age of faulting; iv) the role of faults in determining local seismicity.

The main results document a shear zone, at least 3 km wide, formed by NE-trending fault segments that interrupt coeval NW-trending normal faults. The NE-trending faults controlled the location of the thermal springs and the development of travertine deposits since the latest middle Pleistocene. The thermal springs are still active and travertine is depositing in a slope system, thus suggesting that the activity of the geothermal system is triggered by faulting, as also supported by the widespread low-magnitude seismicity (e.g. seismic events occurred during March 2018; INGV: http://cnt.rm.ingv.it/).

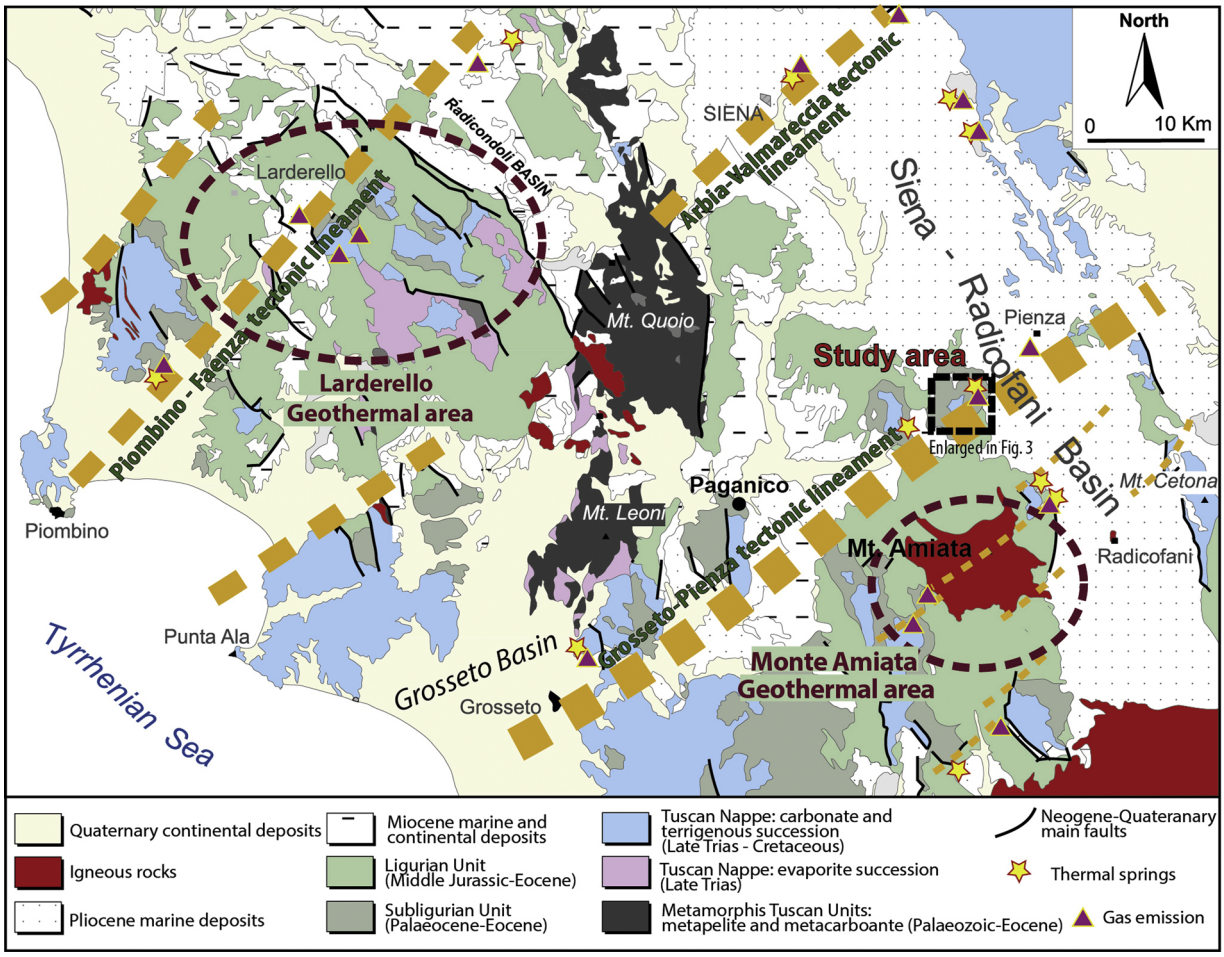


**Fig. 2.** Geological map of the area indicated in Fig. 1, highlighting the main transfer zones associated to Neogene-Quaternary extensional tectonics, the main thermal springs and gas emission (steam, $CO_2$ and $H_2S$); the Larderello-Travale and Monte Amiata geothermal areas are also highlighted. The study area, located along the Grosseto-Pienza tectonic lineament, is indicated by the black rectangle, and it is enlarged in Fig. 3.

## 2. Geologic setting

The Northern Apennines originated from the convergence and collision in the late Cretaceous–early Miocene between the Adria promontory (of African plate pertinence) and the European plate, represented by the Sardinia–Corsica massif (Molli, 2008, and references therein). This process gave rise to the stacking of several tectonic units deriving from different palaeogeographic domains (Vai and Martini, 2001). From the top, the units are (Carmignani et al., 1994): (a) the Ligurian Units, derived from the Ligurian-Piedmont Domain, and consisting of remnants of Jurassic oceanic crust and its late Jurassic-Cretaceous, mainly clayey, sedimentary cover; (b) the Sub-Ligurian Units (Sub-Ligurian Domain), made up of Cretaceous-Oligocene turbidites; (c) the Tuscan Units forming a duplex system and composed of HP metamorphic and sedimentary units ranging from Palaeozoic to early Miocene in age (Pandeli et al., 1991; Carmignani et al., 1994; Rossetti et al., 2002; Brogi and Giorgetti, 2010, 2012).

After nappe stacking, an eastward migrating extension (e.g. Boccaletti et al, 1971; Lavecchia, 1988; Patacca et al., 1990; Doglioni, 1991; Martini and Sagri, 1993; Carmignani et al., 1995; Liotta et al., 1998; Molli, 2008; Barchi, 2010) affected the inner Northern Apennines (i.e., northern Tyrrhenian Sea and Tuscany) from the early–middle Miocene onward (Jolivet et al., 1990; Storti, 1995; Carmignani et al., 1995; Pascucci et al., 1999; Brunet et al., 2000). Although extension was a continuous process through time (Brogi et al., 2005a, 2005b), two main stages can be described. The oldest extensional event occurred during the Miocene (Carmignani et al., 1995; Dallmayer and Liotta, 1998; Brogi and Liotta, 2008; Brogi, 2011) and determined the development of mainly eastward dipping normal faults. Fault development produced: (a) the lateral segmentation of the more competent levels within the previously stacked tectonic units (Decandia et al., 1993); (b) the consequent westward rotation of their hangingwalls and development of bowl-shaped tectonic depressions where Miocene continental to marine sedimentation occurred (Brogi, 2004a; Brogi and Liotta, 2008); (c) the direct superimposition of the Ligurian Units on the late Triassic evaporite and/or on the Palaeozoic phyllite, both representing regional detachment levels (Dallmayer and Liotta, 1998; Brogi and Liotta, 2008); and (d) extension of at least 120% (Carmignani et al., 1994; Brogi, 2006). The younger event (Dallmeyer and Liotta, 1998; Barchi, 2010) has been active since the Pliocene (Fig. 1). This phase of extension is characterized by NW-striking normal faults crosscutting the previously developed structures (Calamai et al., 1970; Lazzarotto and Mazzanti, 1978; Mazzanti, 1966), and defining tectonic depressions where Pliocene-Quaternary marine to continental sediments were deposited (Bossio et al., 1993; Martini and Sagri, 1993; Liotta, 1996; Brogi et al., 2013). These depressions were coeval with NE-trending transfer zones (Liotta, 1991), along which magmatic activity is concentrated (Acocella and Funiciello, 2002, 2006; Dini et al., 2008; Brogi et al., 2010a; Liotta et al., 2015). The amount of extension associated to this event is estimated to be about 6–7% (Carmignani et al., 1994).

This extensional setting and evolution has been confirmed by many field and laboratory studies (Lavecchia, 1988; Jolivet et al., 1990; Carmignani and Kligfield, 1990; Serri et al., 1993; Carmignani et al., 1994, 1995; Liotta et al., 1998; Barchi, 2010; Barchi et al., 1998;

Gualtieri et al., 1998; Negredo et al., 1999; Liotta and Ranalli, 1999; Rossetti et al., 1999; Brunet et al., 2000; Di Bucci and Mazzoli, 2002; Pera et al., 2003; Pauselli et al., 2004; Lavecchia et al., 2004; Molli, 2008; Bartole, 1995; Pascucci et al., 1999; Collettini et al., 2006; Dini et al., 2008; Brogi, 2008b). Alternative interpretations of the tectonic setting and evolution have been proposed (Finetti et al., 2001; Finetti, 2006; Bonini and Moratti, 1995; Bonini and Sani, 2002; Bonini et al., 2014), but an extensional framework better explains the tectonic setting of southern Tuscany as discussed in many papers (e.g. Brogi et al., 2005a, 2005b; Brogi and Liotta, 2008; Brogi, 2011).

In this study, we focus on the Bagno Vignoni area (Figs. 2 and 3), located along the transfer zone named as "Grosseto-Pienza tectonic lineament", affecting the western shoulder of the Neogene Siena-Radicofani Basin (Fig. 2). This basin consists of a broad Neogene NNW–SSE oriented tectonic depression where Pliocene marine sediments are unconformably overlain by Quaternary continental deposits (Bossio et al., 1993; Liotta and Salvatorini, 1994; Pascucci et al., 2007).

In the basin shoulders, the Ligurian Units, Subligurian Units, and the Tuscan Nappe are widely exposed (Fig. 2). Concerning the stratigraphic and tectonic setting of the Bagno Vignoni area, information was given by Losacco (1959) and more recently by Brogi et al. (2005c, 2007) who highlighted duplex structures affecting the Tuscan Nappe, later delaminated during the extensional tectonics. A part of the duplex system is exposed close to Bagno Vignoni locality (Fig. 3) while the remaining part has been drilled (at least in part) by boreholes during exploration for thermal waters (Brogi et al., 2005c; 2007). The duplex structure characterising the Tuscan Nappe reconstructed by boreholes and new fieldwork (illustrated in the next paragraph) is illustrated in Fig. 4.

## 3. Methods

In order to (i) reconstruct the age, geometry and kinematics of faults and (ii) characterize the geochemical features of the palaeofluids (i.e. stabile isotopic composition and temperature), we carried out integrated geological, geochemical and geochronological analyses in the area comprising the Bagno Vignoni travertine deposits (Fig. 3).

First, we conducted new fieldwork focused on geologic mapping of an area of about 10 $km^2$ at 1:5.000 scale (Fig. 3). The first aim of this work was to get information on the factors that controlled, and are still controlling, the hydrothermal fluids flow and travertine deposition. Furthermore, in order to reconstruct the interplay between tectonic activity and travertine deposition we have studied the travertine bodies, in terms of: i) morpho-structural and architectural setting; ii) facies analyses; iii) structural and kinematic setting. Moreover, a geochemical study, in terms of stable and clumped isotopes, and U-Th dating have been performed on the travertine deposits for better constrain the fluids provenience and age of deposition (i.e. faulting).

## 4. Results of geological, geochemical and geochronological analysis

The following sections describe in different paragraphs our new observations of: i) the stratigraphic features of the travertine substratum and structural setting of the area; ii) the architecture of the travertine bodies; iii) stable- and clumped isotope analyses; and iv) geochronological analyses.

### 4.1. Stratigraphy of the travertine substratum and structural setting

We analysed the travertine substratum where it is exposed along the valley of the Orcia River (Fig. 3) that runs orthogonally with respect to the western margin of the Siena-Radicofani Basin. The travertine substratum consists of: (i) late-Triassic-Oligocene sedimentary rocks belonging to the Tuscan Nappe; (ii) Eocene-Oligocene carbonate-terrigenous succession belonging to the Subligurian Unit; iii) Cretaceous carbonate and terrigenous succession belonging to the external Ligurian Units (S.Fiora Unit); and iv) Jurassic-Cretaceous ophiolite-bearing carbonate-terrigenous succession belonging to the inner Ligurian Units (Ophiolitic Unit). Fig. 4 summarizes the stratigraphic logs and the tectono/stratigraphic relationships among the different units. All these units are unconformably overlain by Pliocene marine sediments and, locally, by travertine deposits.

The pre-Neogene units experienced poliphased tectonic deformation during the Cretaceous-early Miocene collisional and Neogene-Quaternary post-collisional evolution of the inner Northern Apennines. Contractional structures (i.e. thrusts, reverse faults, folds and shear zones) affected the pre-Neogene Units to form a tectonic pile (Fig. 4), partially exposed nearby the travertine quarries (Fig. 3), and mostly drilled in the surroundings of the main active thermal springs (Brogi et al., 2007). Nevertheless, due to the effects of the middle-late Miocene extensional tectonics, the Ligurian Units normally rest on the basal part of the Tuscan succession (i.e. late Triassic evaporite), or on different units within the carbonate and terrigenous succession (Fig. 3). Tectonic omissions within the Ligurian and Sub-Ligurian Units also occur frequently within the whole study area (Fig. 3).

Pre-Neogene units and the Neogene-Quaternary deposits, as well as thrusts and extensional detachments, are dissected by two high-angle fault systems (Fig. 3): (i) NE-trending faults, showing left-lateral oblique-slip and normal movements, and (ii) NW-trending faults characterised by dominant normal movements. NE-trending faults consist of anastomosed fault segments, up to 2 km long, that cross the whole area forming an about 3 km wide shear zone: these are characterised by ~ten-meter offsets, and gave rise to the narrow structural depression where the Orcia River developed (Fig. 3). At the cartographic scale, NE-trending faults interrupt the lateral continuity of the NW-trending faults (Fig. 3) and dissect both Neogene sediments and travertine deposits, highlighting that these structures were active during the Neogene and Quaternary. The NW-trending faults display ten-meter offsets and juxtapose early Pliocene marine sediments with the Ligurian Units (Fig. 3). In contrast, in the surroundings areas NW-trending faults are buried by late Pliocene sediments (cf. Liotta, 1994; Pascucci et al., 2006, 2007; Brogi, 2011), suggestion that activity pre-dated the early Pliocene.

Faults affecting the travertine substratum show offsets not exceeding 50 m (Fig. 3) and have core-zones no larger than 5 m (Fig. 5a-e), consisting of brecciated and comminuted rocks (Fig. 5f). Well-developed fractures, in some cases filled by calcite (Fig. 5), define the damage zones, in both the fault walls (Fig. 5c-e). The fault slip-planes often contain mechanical striations and/or calcite/Fe-hydroxides slickensides. Meso-faults affecting the Neogene deposits show displacements occasionally exceeding 10 m (Fig. 5).

Structural and kinematic analyses were carried out on the carbonate and terrigenous succession of the Tuscan Nappe (Figs. 3 and 4), which is composed of the most favourable lithotypes to record striations. More than 50 kinematic data were collected from 12 structural stations; the results are shown in the diagrams of Fig. 3. Kinematic indicators of the NE-trending fault system show two superposed movements, as reconstructed in few structural stations. The first one is defined by left-lateral oblique-slip movements, while the second movement is characterized by a dominant vertical component (Fig. 5g). Movements characterised by dominant normal components have also been recognized in the NW-trending faults.

### 4.2. Travertine deposits

Travertine deposits have a maximum thickness of about 25 m and consist of two distinct bodies located to the southwest and south of the Bagno Vignoni village (Fig. 3–6). The eastern body is still growing in a restricted area (Fig. 6), where 50 °C thermal water (Pentecost, 1994), drained from the thermal spring feeding the "Bagno Grande" pool (Fig. 6d) is conveyed. In contrast, the western body is a fossil deposit extensively quarried during the 1970's (Fig. 6a).

The three abandoned quarries are characterized by saw-cut walls

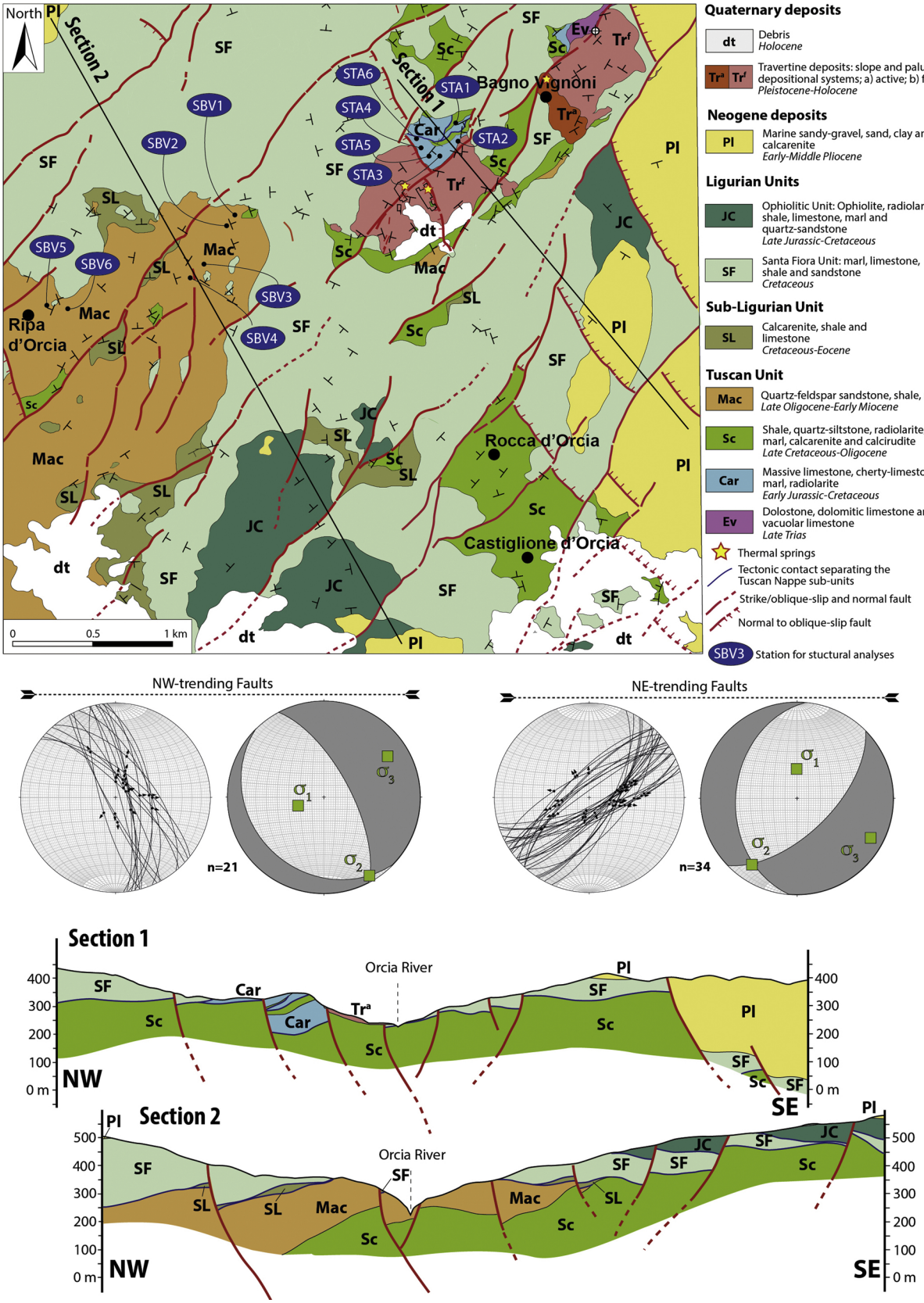


**Fig. 3.** Geological map of the study area and geological sections. Stereographic diagrams (equal area, lower hemisphere) illustrating faults and striae, kinematic axes and fault plane solutions, divided per fault-trends and obtained from the inversion of kinematic data collected on fault-slip surfaces, are also shown.

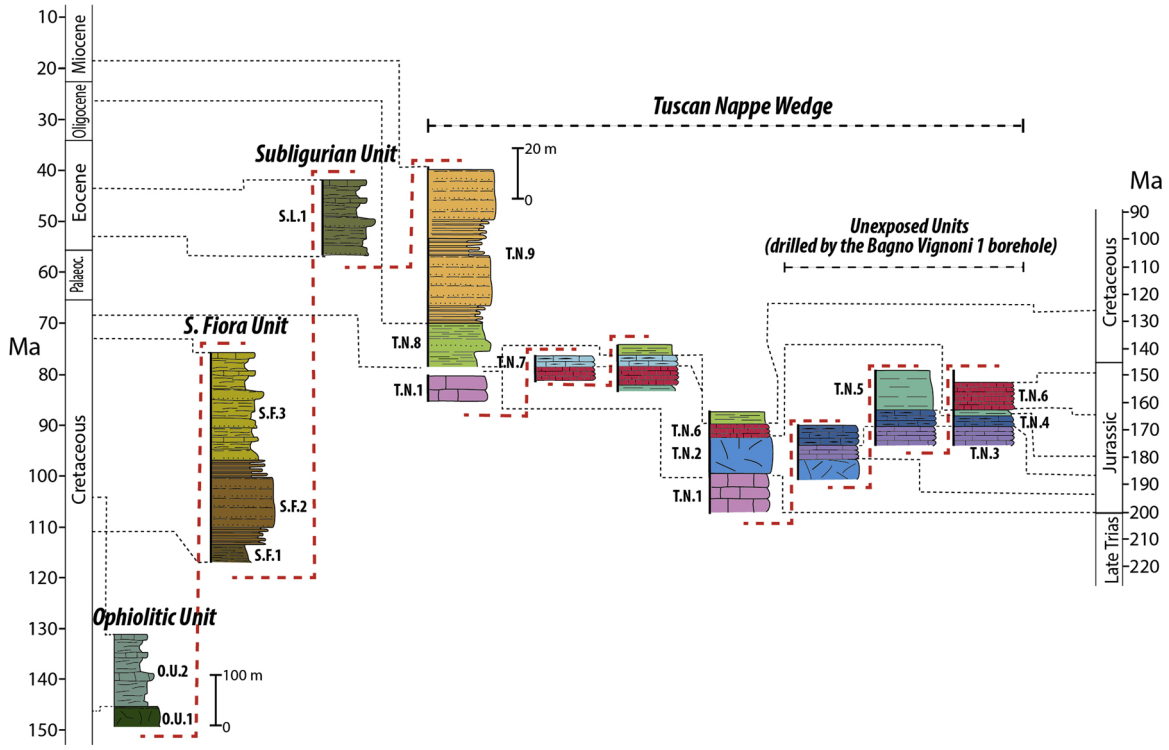


**Fig. 4.** Stratigraphic logs of the tectonic units exposed (and drilled) in the study area, reconstructed through field work and borehole data (Bagno Vignoni 1 borehole in Brogi et al., 2007). Symbols: O.U.1 - Ophiolite (Middle-Late Jurassic); O.U.2 - sedimentary cover represented by siliceous limestone, calcarenite, marl with interbedded shale (Calcari a Calpionella and Argille a Palombini Fms; Early Cretaceous); S.F.1 - Shale, marl, siliceous limestone and radiolarite (Sillano Fm, Early Cretacous); S.F.2 - Sandstone, shale and mal (Pietraforte Fm, Cretaceous); S.F.3 - limestone, marl and shale (Santa Fiora Fm., Cretaceous). S.L.1 - calcarenite, siliceous limestone, shale (Argille e Calcari Fm; Eocene-Oligocene); T.N.1 - Dolostone and dolomitic limestone (Burano Fm, Late Triass); T.N.2 - Massive limestone (Calcare Massiccio Fm., Early Lias); T.N.3 - reddish nodular limestone and shale (Rosso Ammonitico Fm, Middle Lias); T.N.4 - Cherty limestone, marl and shale (Calcare Selcifero Fm., Middle-Late Lias); T.N.5 - Marl and marly limestone (Marne a Posidonia Fm, Dogger); T.N.6 - radiolarite (Diaspri Fm., Malm); T.N.7 - Cherty limestone and marl (Maiolica Fm, Early Cretaceous); T.N.8 - Shale, marl, radiolarite, siliceous limestone, calcarenite and calcirudite (Scaglia Toscana Fm., Late Cretaceous-Late Oligocene); T.N.9 - Quartz-feldspar sandstone, siltstone and shale (Macigno Fm, Late Oligocene-Early Miocene).

allowing the reconstruction of the internal architecture and different depositional events, as well as the location of the feeder conduits of the palaeothermal springs. For this reason, we have studied in detail the westernmost deposit.

In the following, we describe: i) architecture and lithofacies characterising the travertine body and its depositional units; ii) the geometrical setting and textural features of the banded calcite veins; iii) the results of stable- and clumped isotope analyses; iv) the geochronological analyses for age determination.

*4.2.1. Architecture and lithofacies of the travertine deposit*

On the top of the travertine deposits, NW- and NE-trending fissure ridges and cone-shape mounds are aligned along the main faults (Fig. 6a), suggesting a structural control on their location. A NW-trending fissure-ridge (Fissure ridge A, in Fig. 7), 56 m long, bounds the western slope of the Poggione hill (Fig. 6a); the ridge is characterized by a central fissure ranging from 1 to 80 cm in width (Fig. 7). A few tens of meters to the NW limit of the ridge, a cone-shape mound up to 50 cm high indicates the presence of an isolated palaeothermal spring developed along the same fault that controlled the development of fissure ridge A. Another fissure ridge, NW-trending and 60 m long (fissure ridge B, Fig. 7), occurs to the south of the Poggione hill and delimits the eastern saw-cut wall of Quarry 2 (Figs. 6 and 7). The geometry of the bedded travertine is exposed in the westernmost wall of fissure ridge B along its entire length (at least 80 m).

Decimeter-high cone-shape mounds are aligned along the south-eastern slope of the Poggione hill (Fig. 6) for at least 100 m, revealing the geometry of the fault that fed the hydrothermal fluids from which the eastern part of the travertine deposit originated. These mounds are partly dismantled but their occurrence is indicated by up-ward cone-shape travertine beds.

Other minor fissure ridges characterise the whole travertine deposit (Fig. 6). Among these, fissure ridge C (Fig. 6) is exposed in a small saw-cut wall showing the internal architecture of the ridge; our observations show that it is characterized by several superposed lenticular/dome-shaped bedded travertine bodies and corresponding to different depositional phases. The banded calcite vein corresponding to the feeder conduit, active during the latest travertine deposition, is also recognizable (Fig. 8). This evidence indicates the shifting of the feeder fissure through time, therefore implying continuous tectonic activity during travertine deposition.

The quarried travertine deposit (westernmost in Fig. 6a) corresponds to a slope depositional system that passed to a distal zone characterised by sub-horizontal morphology and low-energy environment (Fig. 9a); the whole deposit was fed by thermal springs developed on the NW- and NE-trending fissure ridges and mounds. In this scenario, laminated abiotic crystalline crusts, interrupted by small ponds of microbial mats (Fig. 9b), formed where fluids run along slopes (cf Alçiçek et al., 2017), close to the paleo-thermal springs. In the distal parts, fluids fed palustrine environments, where travertine deposited in vegetated areas (Fig. 9c–d). The increasing amount of vegetation in the distal parts of the deposits suggests the cooling and shifting of the flow system waters.

Travertine deposition was discontinuous through time, as highlighted by the numerous unconformities that separate different depositional events, in some cases accompanied by palaeosoils. Nevertheless, the resulting travertine deposits can be estimated to be a maximum of about 25 m thick.

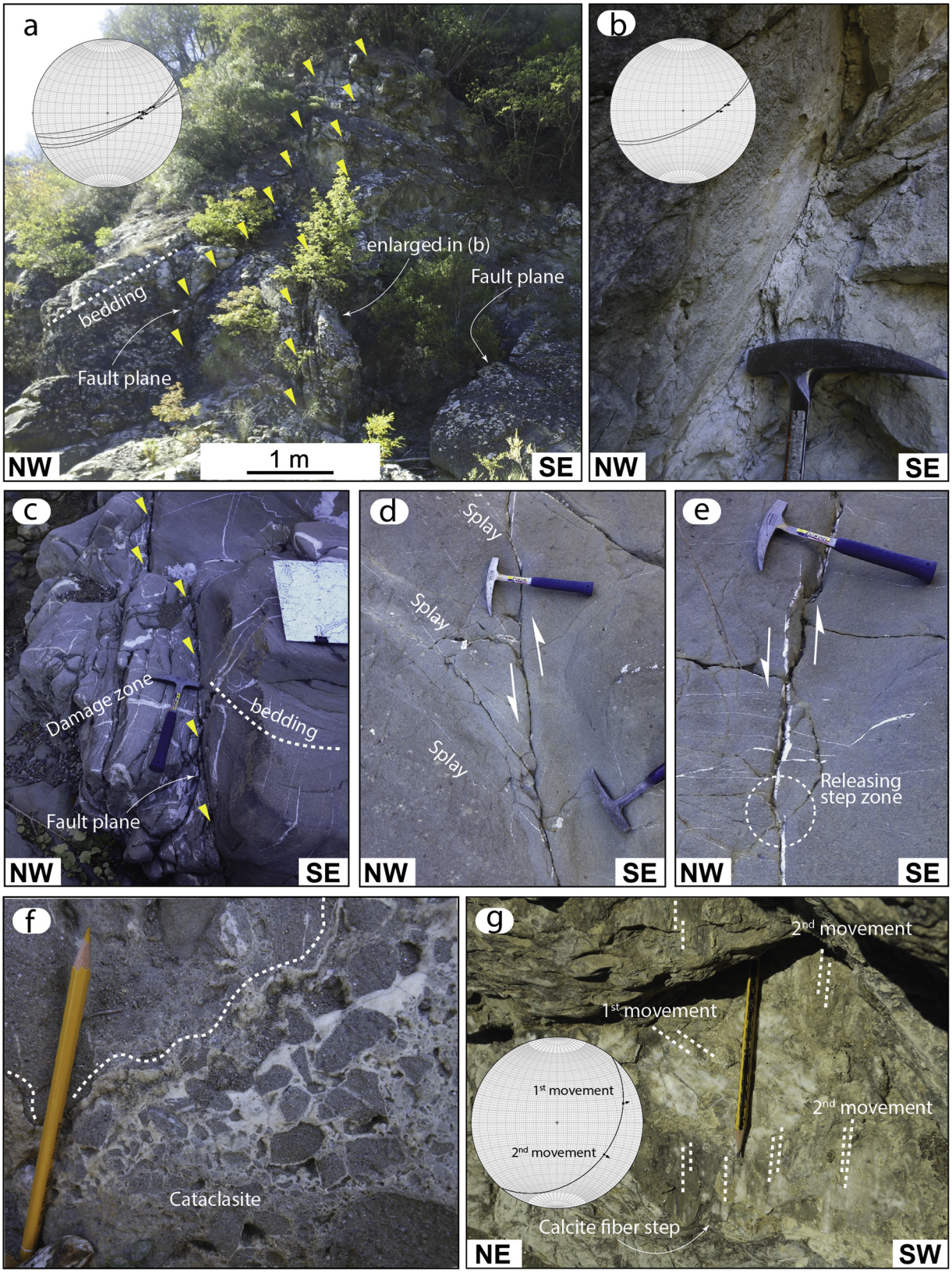


**Fig. 5.** Examples of faults and related minor structures; a) a main fault zone affecting the Macigno Fm along the Orcia River, with offset exceeding 10 m; b) particular of the slip surface and core zone; c) example of damage zone associated to a meter offset fault affecting sandstone beds belonging to the Macigno Fm.; d–e) strike-slip faults, associated splay and extensional jogs developed in releasing step-over zones, representing a minor structure associated with the main transfer zones; f) detail of a permeable cataclasite, presently cemented by calcite, developed in the core zone of a normal fault; g) example of superposed kinematic indicators as recognised in rare fault planes; slickensides are made up of calcite.

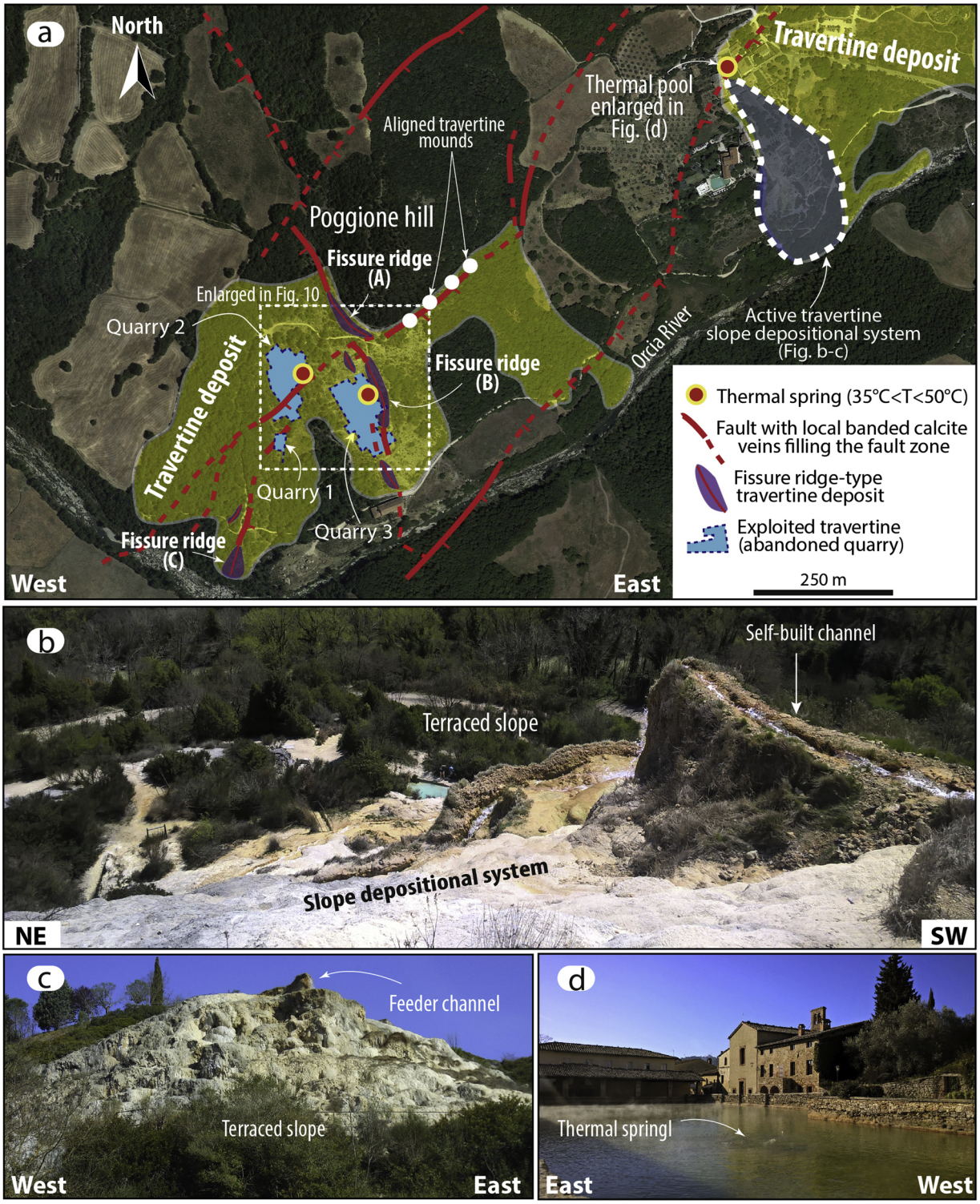


**Fig. 6.** a) Satellite photograph (from Google Earth) illustrating the Bagno Vignoni travertine deposits and the main faults (see also Fig. 3). Fissure ridge-type travertine deposits (A, B and C correspond to fissure ridges described in the text), thermal springs and the abandoned quarries are also reported; b–c) panoramic views of the active travertine slope-depositional system occurring nearby the SPA; d) main thermal spring feeding the Medieval pool and giving rise to the travertine deposition.

Four main lithofacies association (LF1-4 in Fig. 9), assembled in twelve main unconformity-bounded stratigraphic units (S.U0-S.U11 in Fig. 10), have been categorised through the analyses of the quarries saw-cuts:

1 Laminated porous microbialites (LF1), consisting of peloidal micritic layers locally with small and very close pores (fenestral porosity) due to the presence of microbial mats and shrubs (Fig. 9c) and/or layers with larger pores (mouldic porosity) due to the presence of paper-thin raft, bubbles, puffy pastry-like structures and plant imprints (Fig. 9d). Their thickness varies from 0.5 cm to 10 cm. Some units show high porous lens, 15 cm thick, mainly characterized by

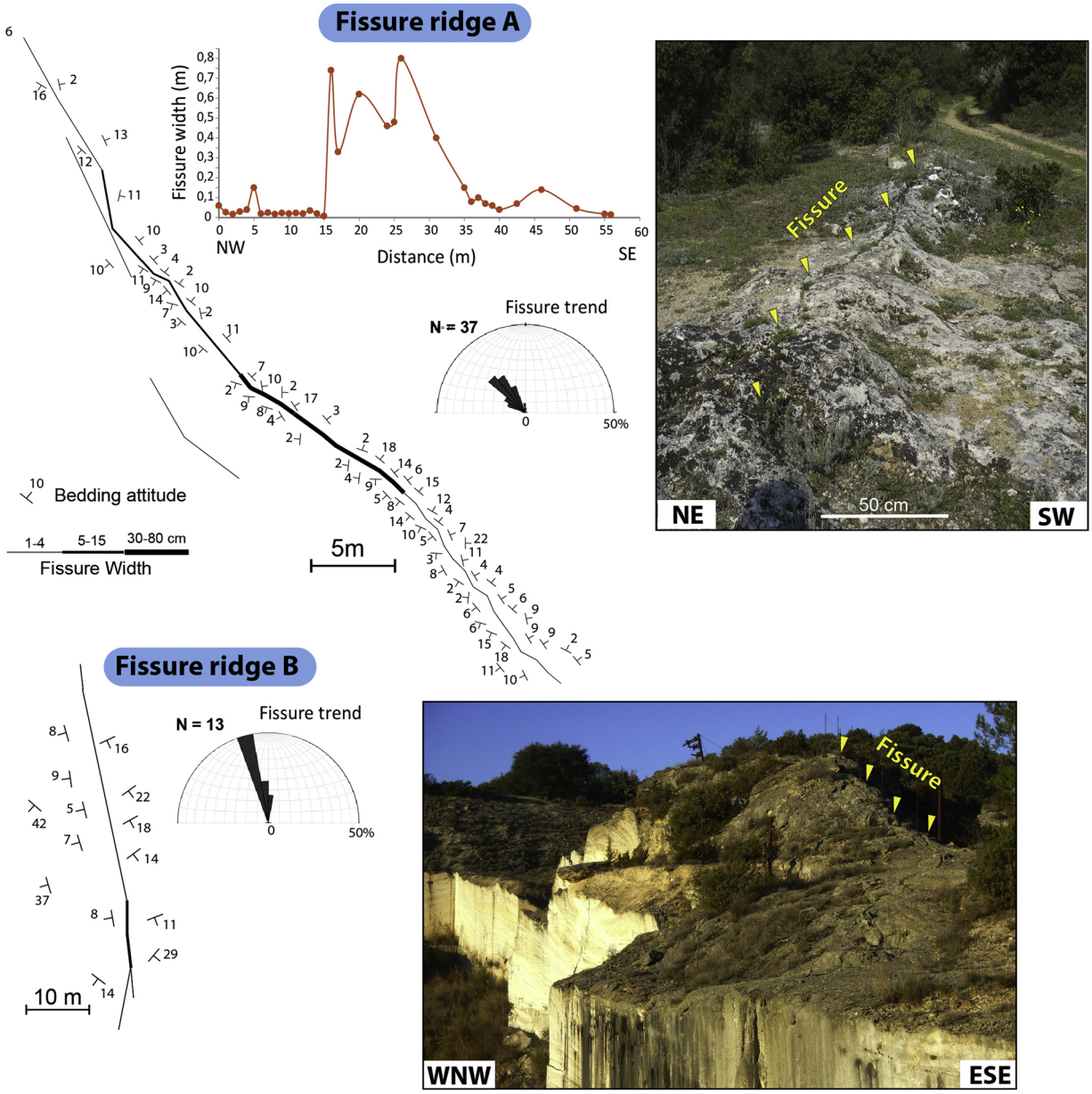


**Fig. 7.** Morphometric analyses and photographs of the fissure ridges A and B (see Fig. 6 and 10 for their location).

microbial mats and also karst cavities partly filled by speleothems. Those kinds of deposits developed far from the slope, in lateral flats and depressions where the water became colder than the source (Guo and Riding, 1999; Gandin and Capezzuoli, 2014; Erthal et al., 2017).

2 Laminated abiotic crusts (LF2) composed by crystalline layers from 2 mm to 5 cm thick, with variable dips ranging from more than 40° to 10°. The lamination is evident for colour changes, from white to yellow-rose-coloured (Fig. 9b). Feather-like crystals make up the majority of layers and fan/ray crystals are visible in some cases. Micro-terraces and small pools developed along slopes, in the flow direction. Abiotic crust layers are locally interrupted by small microbial mats ponds, shrubs, microbial lime and bubbles. Co-existence of abiotic crusts and micro-terraces are typical deposits of high-flux regime that develop on slopes, close to the thermal springs.

3 Brecciated levels (LF3) made up of angular, cm-to-m-sized travertine clasts in a fine grey carbonate matrix, without a preferential orientation (Fig. 9e). These deposits originated from disrupted travertine beds in small muddy morphological depressions (Gradzinski et al., 2014) or as possible earthquake-triggered soft-sediment deformation structures (seismites - Brogi et al., 2018).

4 Micritic lime deposit (LF4) composed by massive, fine-grained, grey-brownish-colored compact limestone (Fig. 9e), developed in distal, palustrine environment characterized by cool and shallow ponds (Gandin and Capezzuoli, 2014).

According to the classification of Capezzuoli et al. (2014), facies association exposed in the quarried travertine deposit (westernmost in Fig. 6a) corresponds to a slope depositional system that passes to a distal zone characterised by sub-horizontal morphology and low-energy environment (Fig. 9a); the whole deposit was fed by thermal springs developed on the NW- and NE-trending fissure ridges and mounds. In this scenario, laminated abiotic crystalline crusts, interrupted by small ponds of microbial mats (Fig. 9b), formed where fluids run along slopes (cf Alçiçek et al., 2017), close to the palaeo-thermal springs. In the distal parts, fluids fed palustrine environments, where travertine deposited in vegetated areas (Fig. 9c–d). The increasing amount of plants

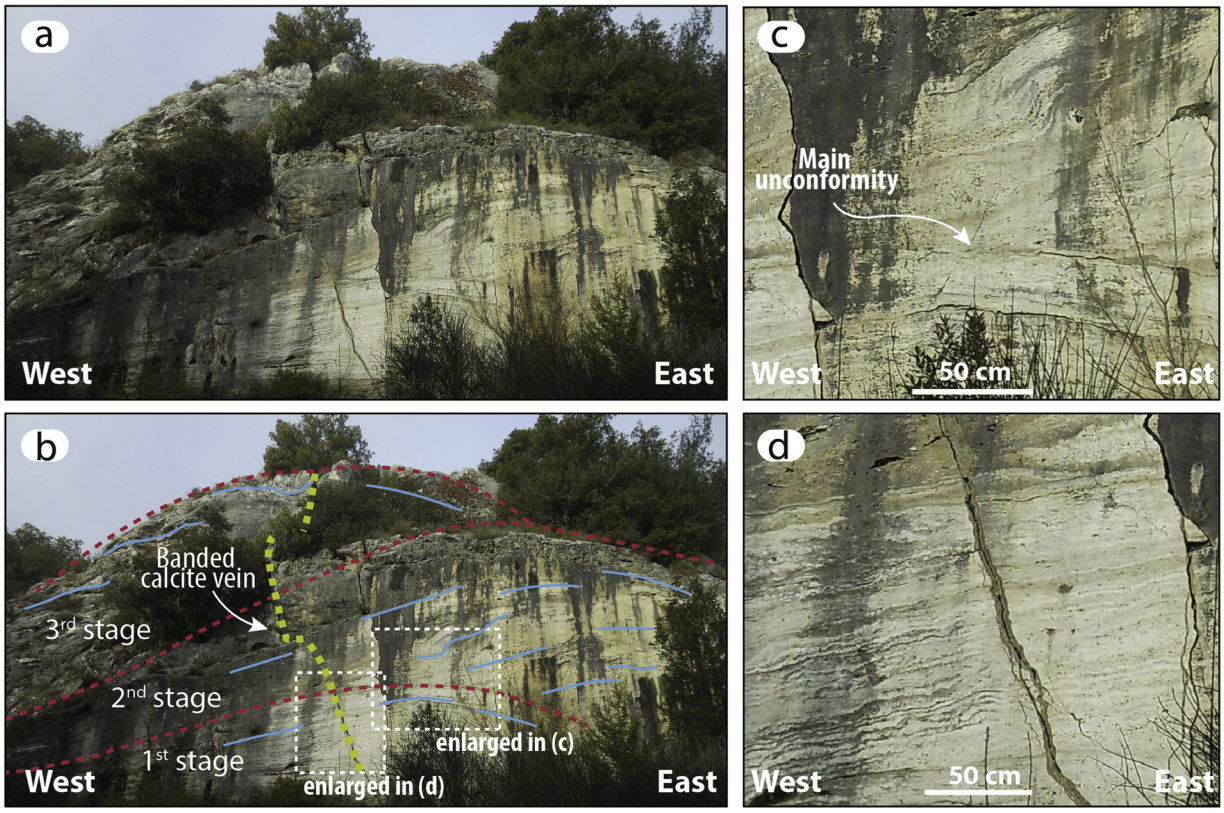


**Fig. 8.** Photographs of the saw-cut wall illustrating the inner part of the fissure ridge C (see Fig. 6 and 10 for its location); a–b) saw-cut wall of the quarry and the line-drawing with the interpretation of the geometrical setting and progressive development; c–d) particular of the angular unconformity and banded calcite vein characterising the travertine body.

in the distal parts of the deposits suggest the cooling and shifting of the waters flow system.

In quarries 1 and 2 the lower travertine units (from S.U0 to S.U5) are exposed (Fig. 10a). These are characterised by gently dipping beds mainly composed of LF1 + LF3 + LF4, indicating a dominant low-energy depositional environment, at least as it concerns the S.U0-S.U3 levels. In Quarry 2, a well-developed palaeosoil, up to 2 m thick, separating the S.U0 from the S.U1 is exposed in the northern saw-cut wall (Fig. 10b). Its occurrence suggests a prolonged depositional stasis, accompanied by erosional processes and pedogenesis, before the deposition of the S.U1 level.

Quarry 3 (Fig. 10) shows most of the travertine succession (from S.U2 to S.U11). Succession from S.U2 to S.U5 is mostly formed by distal (i.e. palustrine: F1 + F3 + F4) facies associations; in contrast, the successions from S.U6 to S.U11 are mainly characterised by proximal (i.e. slope: F2) facies associations developed close to the palaeo-thermal springs located along the fissure ridge B (Fig. 10). The easternmost saw-cut wall shows five depositional units that formed on the western flank of the previously mentioned fissure ridge.

The lower part of the travertine succession (S.U0-S.U3) was dissected by faults. In particular, the S.U0 was strongly dissected by NW-trending faults; deformation affected 10 m of the S.U0 succession as recognised in the western and eastern saw-cut walls of the Quarry 2 (Fig. 11a). Most of tectonic deformation affected the S.U0 and was accompanied by fluid circulation that deposited banded calcite veins in a time-period spanning at least 23.3 ± 0.6 and 9.5 ± 1.8 ka. Several parallel-banded calcite veins cross-cutting each other developed within the fault zones (Fig. 11c–d). The fault zone was partially eroded and buried under the S.U1 (Fig. 11a–d). Nevertheless, faulting continued after the deposition of the S.U1, producing the cracking and tilting of bedded travertine blocks and the development of open fractures, up to 1.5 m in width, filled by bedded travertine (Fig. 11a–b). Such a neoformational travertine was later dissected; banded calcite veins developed along the fault zone therefore suggesting that faulting was accompanied by hydrothermal fluid circulation up to 9.5 ± 1.8 ka (Fig. 11e).

Saw-cut walls of all quarries do not permit us to evaluate if such a fault also dissected the overlying units, even if it is expected.

#### 4.2.2. Geometric and textural features of the banded calcite veins

Most of the banded calcite veins are exposed in the saw-cut walls of the quarries, but in some cases banded veins have also been recognised in the quarry-floors, where the substratum is exposed in restricted windows (Fig. 12a–c). In other cases, banded calcite veins filled the central fissure of minor fissure ridges or have been recognised crossing the travertine beds outside the quarries (Fig. 12d–e). In all cases, the banded calcite veins are NW- and NE-trending, parallel to the main faults recognised in the whole area (Fig. 10a). Veins crosscut each-other and define volumes of deformed travertine beds with a concentrated vein network. In some cases, the chronological relationships among veins are clear but in other cases veins are mutually cross-cutting, defining very complex vein arrays Fig. 11.

Each vein consists of millimeter thick, parallel and/or subparallel vertical crystal bands with different colours: white, grey, yellowish, red and more rarely brownish bands (Fig. 13). In some cases, light-transparent bands have internal black/grey shades. The contact between veins and travertine is sharp. Vein crystals grew normal to the wall-rock, toward the central part of fractures, thus forming symmetrical, isopachous, or less frequent botryoidal mm-to-cm thick crusts (Fig. 13a). Banded veins are commonly sealed although discontinuous voids rimmed by festoons can locally be observed in the central part of the vein.

According to Capezzuoli et al. (2018), Type A bands with elongate-blocky calcite crystals, characterized by 0.17–2.6 mm in length and

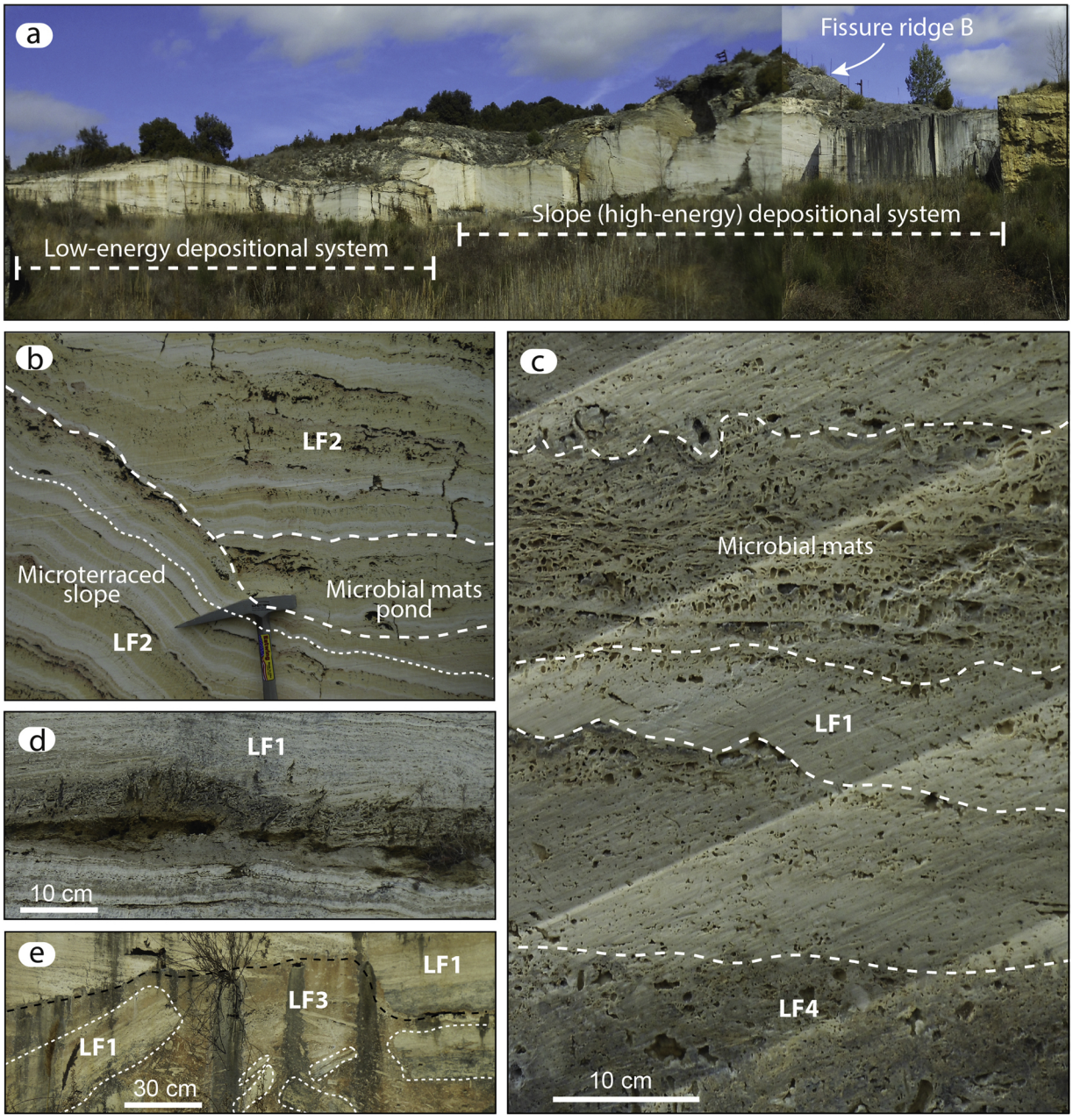


**Fig. 9.** a) Panoramic view of the Quarry 3 where the high- and low-energy travertine depositional environments are highlighted; see the text for more information on the facies distribution and travertine features. b) detail of the lithofacies 2 (as described in the text) typical of running waters along slopes; c) detail of the lithofacies 1 and 4 (as described in the text) developed in low-energy (palustrine) environment; d) example of reed association characterising a travertine level deposited in a palustrine environment; e) detail of the blocks characterising the lithofacies 3 and delimited, at the top, by and erosional surface.

wavy extinction, and Type B bands with microcrystalline (microsparite-to micrite) calcite crystals have been recognised characterising most laminae (Fig. 13b). The Type A elongate-blocky crystals seem to nucleate from Type B microcrystalline cone and grow perpendicular to the vein wall.

*4.2.3. Stable and clumped isotope analyses*

$\delta^{13}C$ and $\delta^{18}O$ analyses have been made on eight key samples (Fig. 10a), some of which used also for radiometric ages determination (Tab. 1). BV 12 and BV 16 are banded calcite veins from Quarry 2 (Fig. 11); BV 10 and BV 11 are respectively from the LF2 and banded calcite vein crossing the S.U1 in the Quarry 2 (Fig. 11e); BV 15 is a LF2 crystalline crust bedded travertine collected SW to the Quarry 3; BGV 8 consists of a LF2 crystalline crust collected close to the previous sample. BGV 7 is a LF1 microbial mat collected in the Quarry 3 and BV 13 is LF2 crystalline crust located in Quarry 2. See Figs. 10a and 11 for their location.

Stable carbon and oxygen isotope measurements were performed on powders at the Institute for Geological and Geochemical Research, Hungarian Academy of Sciences, Budapest, Hungary, using the continuous flow technique with the $H_3PO_4$ digestion method (Spötl and Vennemann, 2003). $^{13}C/^{12}C$ and $^{18}O/^{16}O$ ratios of $CO_2$ generated by acid reaction were measured using a Thermo Finnigan Delta Plus XP continuous flow mass spectrometer equipped with an automated GasBench II. The results are expressed in the δ-notation [$\delta = (R1/R2 - 1) \times 1000$] where R1 is the $^{13}C/^{12}C$ or $^{18}O/^{16}O$ ratio of the sample and R2 is the corresponding ratio of the Vienna Pee Dee Belemnite (VPDB) standard, in parts per thousand. Finnigan Delta Plus XP continuous flow mass mean values are given in the standard δ-notation in parts per thousand (‰) relative to VPDB ($\delta^{13}C$ and $\delta^{18}O$) and Vienna Standard

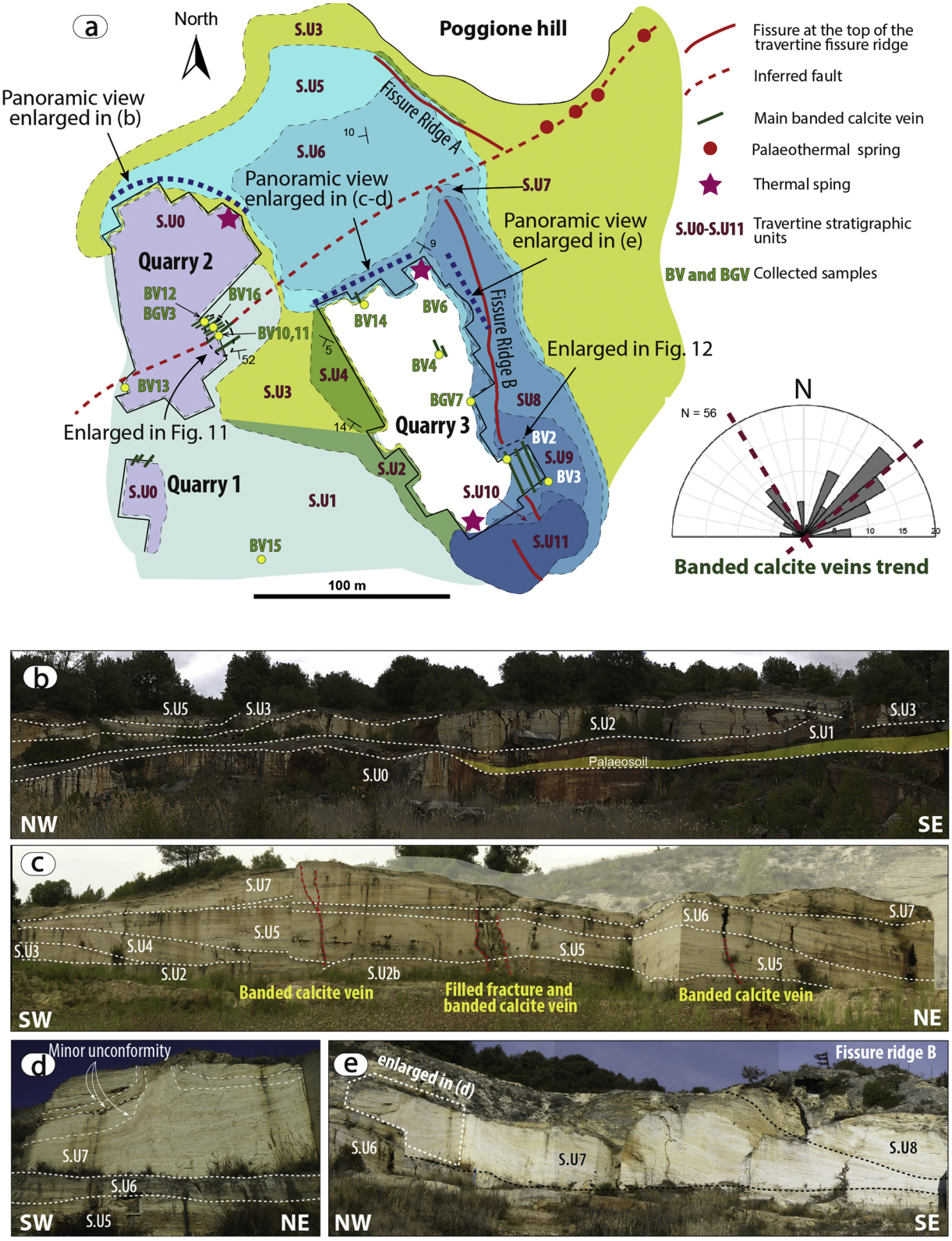


**Fig. 10.** a) Sketch-map of a part of the western travertine deposit (see Fig. 6 for its location) where the abandoned quarries are located. The twelve Stratigraphic Units (S.U.0–11) are indicated with different colours. The location of the banded calcite veins, palaeothermal springs forming mounds and fissure ridges are also reported. b) panoramic view of the northern wall of the Quarry 2, where the S.U0-S.U5 have been described; c–d) panoramic view of the northern wall of the Quarry 3, where the S.U2-S.U7 have been described; e) panoramic view of the eastern wall of the Quarry 2, where the S.U7-S.U8 forming the western slope of the fissure ridge B are exposed.

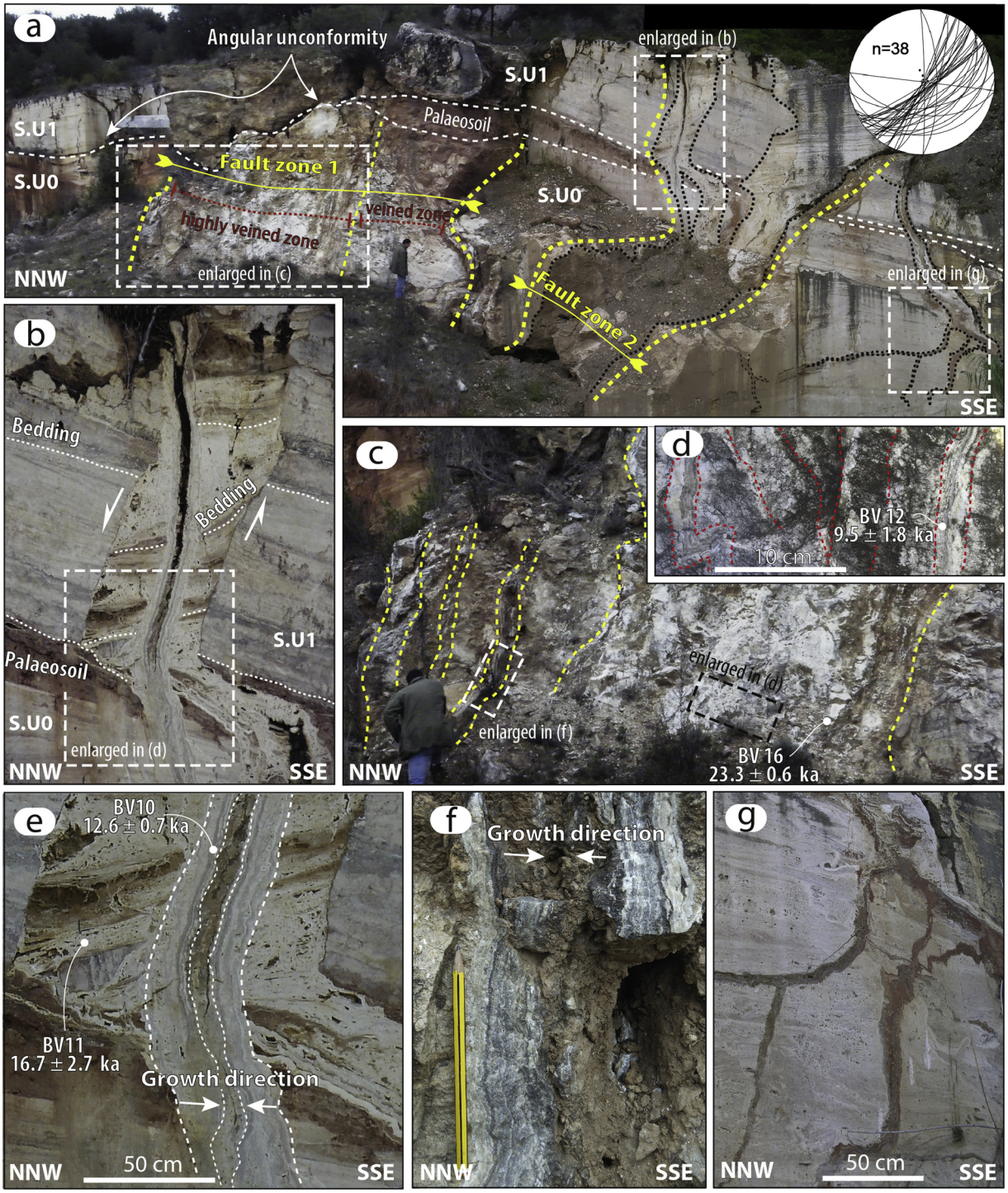


**Fig. 11.** Particular of fault zones filled by banded calcite veins exposed in the eastern saw-cut wall of the Quarry 2 (see Fig. 10 for location); a) panoramic view of the fault zones and banded calcite veins. Note how the fault zone 1 affected only the S.U0; on the contrary, fault zone 2 dissected both S.U0 and S.U1. b) particular of the fault zone 2 highlighting a fracture affecting the bedded travertine, filled by bedded travertine lithons travertine and dissected again during a hydrothermal fluids circulation that deposited the banded calcite vein; c–f) particular of the banded calcite veins filling the fault zones; e) fractures filled by calcite and paleosoil affecting the bedded travertine of the S.U0. Ages are also reported and indicated in Table 3.

Mean Ocean Water (VSMOW; $\delta^{18}O$). Duplicates of standards and samples reproduced values.

Results of the carbon and oxygen isotope compositions of all samples are reported in Table 2 and Fig. 14. $\delta^{13}C$ and $\delta^{18}O$ values range between 2.27 and 3.76‰ and between 20.23 and 22.51‰, respectively. The $\delta^{13}C$ and $\delta^{18}O$ values for the bedded travertine samples BV13 and BV11 differs from the others and show the lowest $\delta^{13}C$ values and the highest $\delta^{18}O$ values. The $\delta^{13}C$ values of the banded travertines are high (between 3.54 and 3.76‰), while their $\delta^{18}O$ values vary between 20.23 and 22.17 $\delta^{18}O$‰.

The clumped isotope measurement was applied to a sample consisting of a banded calcite vein (BV 10), collected in the Quarry 2, (Figs. 10 and 11), in order to reconstruct the palaeotemperature of the hydrothermal fluids that were channeled thought the faults. The same

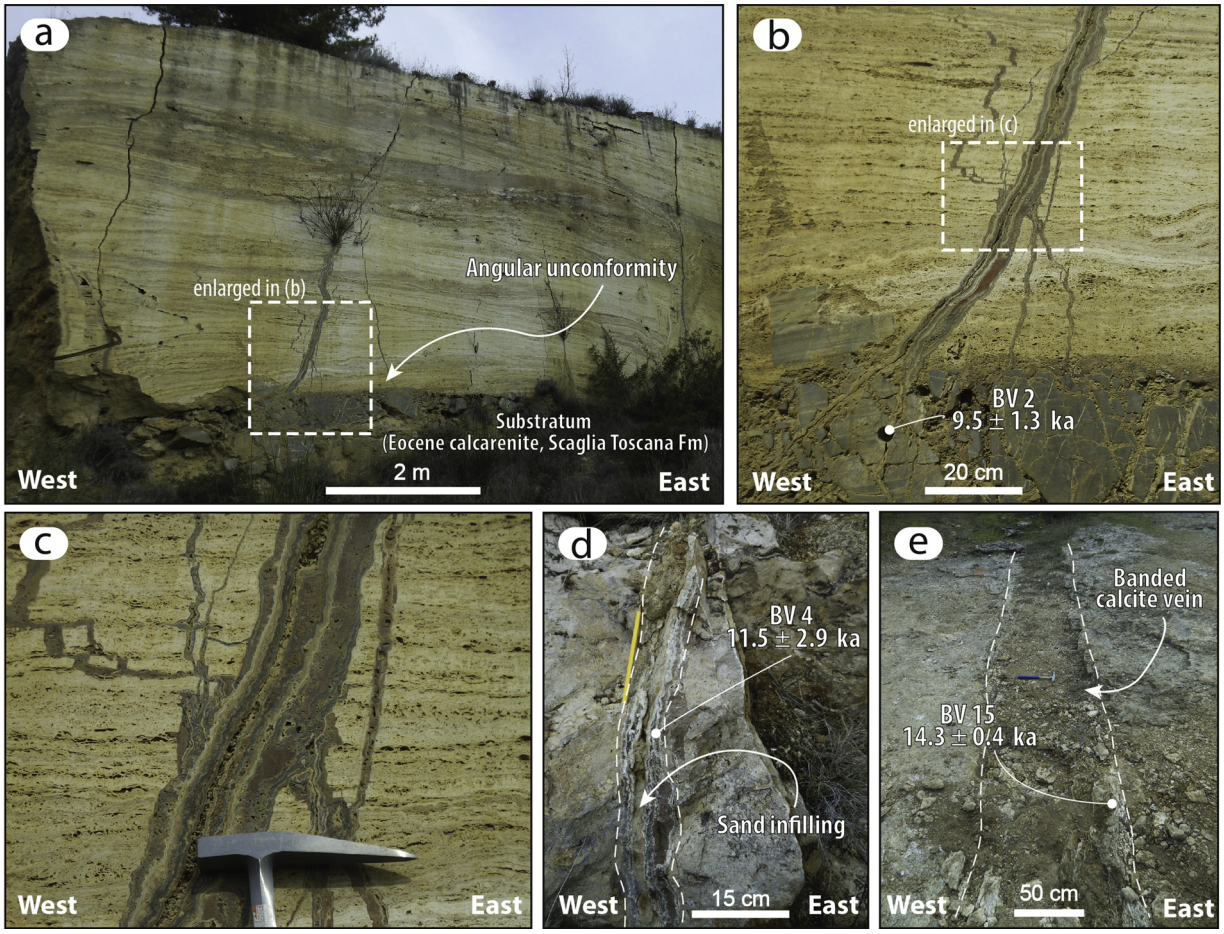


**Fig. 12.** a–c) Particular of the saw-cut wall of the Quarry 3 (Fig. 10 for the location) showing a banded calcite vein crossing the travertine deposit and its substratum, made up of Late Eocene calcarenite belonging to the Scaglia Toscana Fm. d–e) example of banded calcite veins crossing the banded travertine outside of the quarries. Ages are also reported and indicated in Table 3.

sample was also analysed through U-Th radiometric dating (see the next paragraph). The powder sample (2 aliquots of BV 10, each 6 − 8 mg) were analysed at the IsoLab, University of Washington, Seattle, WA, USA, using the procedures of Burgener et al. (2016); Schauer et al. (2016) and Kelson et al. (2017). Powdered calcite was reacted in a common acid bath at 90 °C and purified using an automated system. Purified $CO_2$ was analysed using a Thermo MAT253 isotope ratio mass spectrometer. Following Schauer et al. (2016), IUPAC parameters were used to correct for $^{17}O$ interference (Brand et al., 2010). Pressure baseline correction (He et al., 2012) was made by measuring the reference gas signal 0.0084 V down voltage of the mass 46 peak centre. Clumped isotope values (Δ47) are referenced to the carbon dioxide

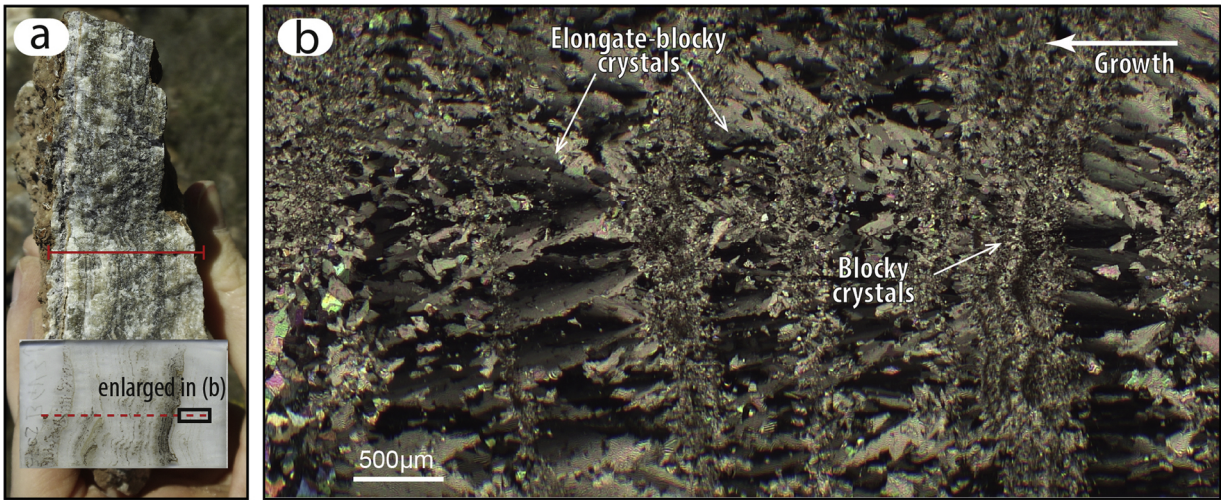


**Fig. 13.** Example of the texture of the banded calcite vein: a) banded calcite vein and thin section across the whole vein in the indicated area; b) thin section (polarized light) showing the fabric of the calcite crystals forming the different bands of the vein; see the text for more information.

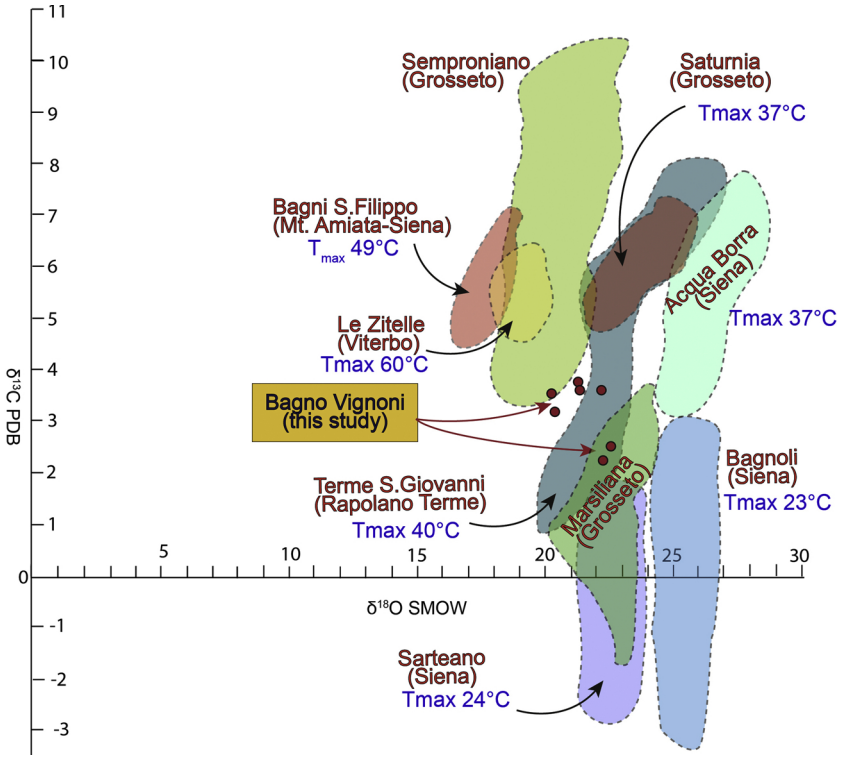


**Fig. 14.** Isotope values of the studied samples compared with samples from other areas characterised by similar settings (see the text for more information); data from: Minissale (2004), Gandin and Capezzuoli (2008), Ricci et al. (2015), Ronchi and Cruciani (2015); Berardi et al. (2016), Croci et al. (2016), Rimondi et al. (2016).

equilibrium scale, or absolute reference frame Δ47 reference frame (Dennis et al., 2011) using $CO_2$ equilibrated at 4, 6 0 and 1000 °C. Temperatures were calculated from measured Δ47 values using the calibration of Kelson et al. (2017), which was generated in the same laboratory as our sample data.

Results of the clumped isotope measurements are summarized in Table 2. The determined average Δ47 value is 0.588 ± 0.021‰. The corresponding temperatures were calculated using of the equation of Kelson et al. (2017) resulting 32 °C. In course of the Δ47 measurement stable oxygen and carbon isotopic values of the samples were also measured (Table 2).

$\delta^{18}O$ of the precipitating water was calculated for the BV10 sample using the temperature dependence of the calcite-water oxygen isotope fractionation (equations of Kim and O'Neil, 1997; Coplen, 2007 and Kele et al., 2015), the $T_{\Delta 47}$ and the $\delta^{18}O_{carbonate}$ values.

#### 4.2.4. U-Th dating

Key samples from the travertine deposit and from the calcite veins of the main fault zones have been collected in the different quarries and surroundings for datings (Fig. 10, Table 1). The age of the bedded travertine deposit has been defined collecting samples from the lower (S.U0) and upper (S.U10) units exposed in the quarries 1 and 3, respectively. The uppermost unit (S.U11) was not sampled as composed by not suitable travertine lithofacies, too altered for analysis. Samples of the banded calcite veins have been collected in order to reconstruct the age of the fluid circulation within the fault zones. We performed U-Th dating analyses using two different techniques: α spectrometry performed at the Laboratorio di Geochimica Ambientale e Isotopica of Roma Tre University (Italy), and Thermo Electron Neptune multi-collector inductively coupled mass spectrometer (MC-ICP-MS) (Shen et al., 2012) at the High-Precision Mass Spectrometry and Environment Change Laboratory (HISPEC) of the National Taiwan University, Taipei (Taiwan ROC).

For α spectrometry, we dissolved around 60 g of sample in 7 N $HNO_3$, filtering the solution to remove the insoluble residue. After adding hydrogen peroxide to destroy organic matter, the leachate was heated at 200 °C and then spiked with a $^{228}Th$–$^{232}U$ tracer. U and Th isotopic complexes were extracted following the procedure described in Edwards et al. (1988) and alpha-counted using high-resolution ion-implanted Ortec silicon-surface barrier detectors. Due to the presence of detrital non-radiogenic $^{230}Th$, ages obtained for samples with a $^{230}Th/^{232}Th$ activity ratio lower than or equal to 50 were corrected assuming an average $^{230}Th/^{232}Th$ activity ratio of 0.85 ± 0.36 (Wedepohl, 1995), which is the crustal thorium mean composition. We then calculated the ages using ISOPLOT, a plotting and regression program for radiogenic-isotope data (Ludwig, 2003).

For MC-ICP-MS dating, about 0.05 g of sample were covered with $H_2O$ and gradually dissolved with double distilled 14 N $HNO_3$. After dissolution, we added a $^{229}Th$–$^{233}U$–$^{236}U$ spike (Shen et al., 2003) to the sample, followed by 0.5 ml of $HClO_4$ to decompose the organic matter. We then followed the chemical procedure described in Shen et al. (2003) for the separation of uranium and thorium for instrumental analysis on MC-ICP-MS (Shen et al., 2012). We calculated the age correction using an estimated atomic $^{230}Th/^{232}Th$ ratio of 4 ± 2 ppm. These latter value is typical for a material at secular equilibrium with the crustal $^{232}Th/^{238}U$ value of 3.8. We arbitrarily assumed a 50% error.

U-Th geochronology results are summarized in Table 3. The age of the travertine deposit ranges from 160.6 ± 6.6 ka to 22.1 ± 5.2 ka as deduced by the analyses of samples BV3 and BV13 (Fig. 10a; Table 3). Samples collected in the banded calcite vein network recognised in Quarry 2 (Figs. 10 and 11) indicate that the S.U0 was affected by faulting ~ 23.3 ± 0.6 ka; faulting deformed the same rock volume and also the overlying S.U1 deposit until 9.5 ± 1.8 ka (Table 3 and Fig. 11), therefore suggesting fault activity during travertine deposition for at least 13 ka. This time span also includes the development of the palaeosoil and the angular unconformity separating S.U0 from the overlying S.U1 deposit (Fig. 11). Other banded calcite veins collected in Quarry 3 and surroundings (Fig. 10a) show ages that are in agreement with this time span, suggesting fault activity comprised between 14.3 ± 0.4 ka and 9.5 ± 1.3 ka (Table 3 and Fig. 10a).

## 5. Discussion

Our discussion is focused on: a) structural setting and tectonic

**Table 1**
Analysed samples: their location is indicated in Fig. 10a.

| Sample | Coordinates | U/Th | Stable Isotope | Clumped Isotope | Type |
|---|---|---|---|---|---|
| BV2 | 43° 1'21.95"N 11°36'39.05"E | X | – | – | Banded Calcite Vein |
| BV3 | 43° 1'21.46"N 11°36'39.48"E | X | – | – | Bedded Travertine |
| BV4 | 43° 1'23.43"N 11°36'37.35"E | X | – | – | Banded Calcite Vein |
| BV6 | 43° 1'24.76"N 11°36'37.49"E | X | – | – | Bedded Travertine |
| BV 10 | 43° 1'23.89"N 11°36'32.42"E | X | X | X | Banded Calcite Vein |
| BV 11 | 43° 1'23.86"N 11°36'32.40"E | X | X | – | Karstic infilling |
| BV 12 | 43° 1'24.16"N 11°36'31.87"E | X | X | – | Banded Calcite Vein |
| BV 13 | 43° 1'23.60"N 11°36'30.18"E | X | X | – | Bedded Travertine |
| BV 15 | 43° 1'16.41"N 11°36'27.90"E | X | X | – | Banded Calcite Vein |
| BV 16 | 43° 1'24.10"N 11°36'31.99"E | X | X | – | Banded Calcite Vein |
| BGV7 | 43° 1'22.76"N 11°36'37.99"E | – | X | – | Bedded Travertine |
| BGV8 | 43° 1'16.22"N 11°36'27.21"E | – | X | – | Bedded Travertine |

control on fluid circulation; b) inferred relationships between travertine deposition and faulting, and their age constraints; and c) consideration of the regional tectonic and seismotectonic setting.

### 5.1. Tectonic control on fluids circulation and travertine deposition

The strict relation among thermal springs, travertine deposition and tectonic activity has been widely documented by several authors in the last decades (Hancock et al., 1999; Altunel and Hancock, 1993a, 1993b; Çakır, 1999; Hancock et al., 1999; Brogi, 2004b; Altunel and Karabacak, 2005; Uysal et al., 2007, 2009; Mesci et al., 2008; Brogi and Capezzuoli, 2009, 2014; Temiz et al., 2009, 2013; Brogi et al., 2010b, 2016; Temiz and Eikenberg, 2011; Alçiçek et al., 2017; Claes et al., 2017; Henchiri et al., 2017; Berardi et al., 2016; Brogi et al., 2017, 2018; Alçiçek et al., 2016, 2018, 2019a, 2019b; Karabacak et al., 2019). These authors underline the role of travertine deposits in recording tectonic activity through time in geothermal areas. Fluid circulation and upwelling overall in geothermal systems (Barbier, 2002) depends on the permeability induced by bedrock fractures (Caine et al., 1996; Cox et al., 2001): interconnection of micro- and macro-fractures control the pathways of hydrothermal fluids (Cox et al., 2001; Zucchi et al., 2017), suggesting that faults related-damage in rock volumes plays a major role in controlling hydrothermal fluids flow in upper crustal levels. Damaging may be enhanced (and therefore fluid flow channelled) where faults link, crosscut each-other, and intersect (Kim et al., 2003), thus influencing the location of thermal springs (Curewitz and Karson, 1997). As previously described, in the study area travertine deposition was (and is) mainly controlled by the NE-striking faults, overall where NE-striking faults intersect the NW-striking ones; in fact, fissure ridges-type travertine deposits and mounds developed along both fault trends and nearby their intersection. Travertine deposition at the intersection of NW (i.e. normal)- and NE (i.e. trasfer)-striking faults is a common feature also for the surroundings areas, as described for the Monte Amiata region (Brogi, 2008a; Brogi and Fabbrini, 2009; Rimondi et al., 2015; Vignaroli et al., 2016), Rapolano Terme area (Brogi, 2004b) and Monte Cetona area (Brogi et al., 2012), as well as worldwide (e.g. New Zeland, Rowland and Sibson, 2004; western Anatolia, Alcicek et al., 2013).

### 5.2. Age of faulting, tectonic activity, palaeofluid temperatures and $CO_2$ origin

Fissure ridges and banded calcite veins occurrence across travertine deposits and substratum present an excellent opportunity for reconstructing the age of faulting (Hancock et al., 1999; Altunel and Karabacak, 2005; Uysal et al., 2007; Karabacak et al., 2019; Török et al., 2019).

Travertine deposition originates from fluids with high sealing capacity that tends to decrease the fault permeability in absence of tectonic activity or seismic events (Muir-Wood, 1993; Curewitz and Karson, 1997; Hancock et al., 1999; Micklethwaite and Cox, 2004; Anderson and Fairley, 2008). As a result, travertine deposition occurs during tectonically active periods (Brogi and Capezzuoli, 2014; Brogi et al., 2018; Karabacak et al., 2019; Williams et al., 2017), if climate is favourable (Faccenna et al., 2008), and the age of travertine deposits can reveal much about the age of faulting (Hancock et al., 1999; Uysal et al., 2007).

The analysis of the internal architecture of the travertine deposits, in terms of geometrical setting of their different depositional units and facies, can provided information for the reconstruction of the original morphology of the travertine body and feeder systems, represented by fissure ridges, mounds and banded calcite veins. Our data indicate that the feeder systems were controlled by both NW- and NE-trending faults delimiting the Poggione hill to the west and south, respectively (Fig. 6). The flowing waters deposited the travertine beds on neighbouring slopes and morphological depressions (Fig. 9).

Banded calcite veins are consequence of crack-and-seal processes (Sibson, 1987), indicative of repeated fracture opening pulses and contemporaneous fluids flow (Altunel and Karabacak, 2005; Uysal et al., 2009; Brogi et al., 2016, 2017; Capezzuoli et al., 2018), accompanied by aragonitic-calcitic laminae deposition. If this view, each lamina forming the banded veins recognised in the Quarries 2 and 3 should be deposited in correspondence of a tectonic pulse, therefore revealing its age. Orientation of the banded calcite veins (NW- and NE-trending) is parallel to the fissure ridges, matching the main faults trend as recognised in the whole study area (Figs. 3 and 6a).

The radiometric ages obtained from the banded calcite veins developed along the NE-striking faults system range from 23.3 ± 0.6 ka to 9.5 ± 1.8 ka, indicating fluids-assisted tectonic activity for at least 13 ka (Figs. 10a and 11, Table 3). The banded calcite veins developed along the NW-trending fault indicate activity between at least 14.3 ± 0.4 ka and 9.5 ± 1.3 (Figs. 10a and 12, Table 3), suggesting that the two fault systems were coeval, at least during the last period of their tectonic activity, with the NE-trending faults documenting a longer history of crack and seal processes. Nevertheless, the age of the travertine deposits suggests that the activity of both fault systems may have initiated earlier: the lower and older depositional unit (S.U0), fed by the NE and NW-trending fissure ridges, have been dated at 160.6 ± 6.6 ka (Tab. 3). This fact suggests that fault permeability and hydrological conditions favoured travertine deposition since the latest middle Pleistocene. It is possible that faults activity started before the travertine deposition giving the tendency of faults to become permeable during their mature stage (cf Caine et al., 1996).

In contrast, deposition of the youngest age of travertine deposit (S.U10) was associated with fluids flow from fissure ridge B that was active until at least 22.1 ± 5.2 ka. Ages of NW-trending banded travertine veins suggest a younger age of fluid circulation, at least until 9.5 ± 1.3 ka.

**Table 2**
Results of the stable and clumped isotopes analyses.

| Sample | $\delta^{18}O_{trav.}$ (‰, V-SMOW) | 1000lnα (using Kim and O'Neil equation, 1997; ‰) | $\delta^{18}O_{water}$ (‰, V-SMOW) | 1000lnα (using Coplen equation, 2007 ; ‰) | $\delta^{18}O_{water}$ (‰, V-SMOW) | 1000lnα (using Kele equation, 2015; ‰) | $\delta^{18}O_{water}$ (‰, V-SMOW) |
|---|---|---|---|---|---|---|---|
| BV10 | 21.24 | 26.67 | −5.43 | 28.45 | −7.22 | 29.54 | −8.30 |
| BV 11 | 22.51 | 26.67 | −4.16 | 28.45 | −5.95 | 29.54 | −7.03 |
| BV 12 | 20.23 | 26.67 | −6.43 | 28.45 | −8.22 | 29.54 | −9.31 |
| BV 13 | 22.23 | 26.67 | −4.44 | 28.45 | −6.23 | 29.54 | −7.31 |
| BV 15 | 21.36 | 26.67 | −5.30 | 28.45 | −7.09 | 29.54 | −8.18 |
| BV 16 | 22.17 | 26.67 | −4.50 | 28.45 | −6.28 | 29.54 | −7.37 |
| | | CLUMPED TEMPERATURE of the BV-10 sample is 32 C. | | | Precise way of calculation: | $\alpha_{c\text{-}w} = (\delta^{18}O_c + 1000) / (\delta^{18}O_w + 1000)$ | |
| | BV-10 | d18O pdb | T (C°) | T (kelvin) | 1000lnalpha, Kim-Oneil (1997) | alpha (Calc-H2O) | d18Owater |
| BV 10 | −9.38 | d18O smow | 32 | 305.15 | 26.66569556 | 1.027021567 | −5.63 |
| | | | | | 1000lnalpha, Coplen (2007) | alpha (Calc-H2O) | d18Owater |
| | | | | | 28.45390791 | 1.028859552 | −6.45 |
| | | | | | 1000lnalpha, Kele (2015) | alpha (Calc-H2O) | d18Owater |
| | | | | | 29.54153695 | 1.029979062 | −8.49 |

Fluid flow and travertine deposition is still active in the eastern side of the study area, along the NE-trending fault system (Figs. 3 and 6). Travertine deposition implies that some faults segments are still permeable; their permeability is possibly maintained by the widespread low-magnitude seismicity recorded in the area (http://cnt.rm.ingv.it/).

Temperature of hydrothermal fluid that circulated within the fault zones, as determined through clumped isotopes method (32 °C) and the $\delta^{18}O$ using the temperature dependence of the calcite-water oxygen isotope fractionation (equations of Kim and O'Neil, 1997; Coplen, 2007 and Kele et al., 2015), is in the range of the Present fluids flowing from the active thermal springs in the Quarry 3. This result suggests that the geothermal system did not change through time, at least considering water temperature. The use of the equation of Kim and O'Neil (1997) resulted -5.63‰, while the use of Coplen (2007) and Kele et al. (2015) resulted lower $\delta^{18}O_{water}$ values (-7.41‰ and -8.49‰, respectively). These calculations demonstrate that the calculated $\delta^{18}O_{water}$ values depend strongly upon the equation used. Kele et al. (2015) noted that in several travertine systems mineral–water oxygen isotope fractionation is usually higher than that computed by the equation of Kim and O'Neil (1997). Thus, $\delta^{18}O_{water}$ it was most probably lower than -5.63‰. The $\delta^{18}O_{water}$ value of the Bagno Vignoni thermal spring is -7.9‰ (Fancelli and Nuti, 1974) and present thermal springs in the area show similar values. Therefore, our isotopic data suggest that the parent fluids of the travertine deposits and banded calcite veins show isotopic composition similar to the present thermal springs. It must be further noted that the $\delta^{18}O_{water}$ values of the present precipitation in the area is about -7‰ (Rimondi et al., 2015). Thus, travertines and banded calcite veins at Bagno Vignoni could have been deposited from meteoric-derived fluids heated by the regional geothermal anomaly. Their uprising, of course, is favoured by the faults-induced permeability.

Based on their positive $\delta^{13}C$ values (Table 2) the studied calcite vein and travertine samples are of thermogene origin using the nomenclature of Pentecost (2005); their $\delta^{13}C$ values might be indicative of the origin of $CO_2$ sources. The use of the empirical equation of Panichi and Tongiorgi (1976) resulted $\delta^{13}C_{CO2}$ values between -7.8 and -6‰ (V-PDB). The theoretical equation of Bottinga (1968) provided similar $\delta^{13}C_{CO2}$ values ranging between -7.1 and -5.7‰ (V-PDB) assuming equilibrium fractionation and using the $\delta^{13}C$ values of travertines and the calculated $T_{\delta 47}$ (32 °C) of the BV 10 sample. The $CO_2$ coming from magmatic sources has generally very low $\delta^{13}C$ values (from −7‰ to −5‰; Hoefs, 1997; Kele et al., 2011), thus our calculations using both equations might indicate a deep, mantle origin for the $CO_2$.

### 5.3. Regional and seismotectonic considerations

The NE-trending faults recognised in the study area define a wide shear zone, up to 3 km wide (Fig. 3) that is part of the transfer zone known as the Grosseto-Pienza tectonic lineament (Fig. 2). This is one of the first order NE-trending (Fig. 1) shear zone described for the inner zone of the Northern Apennines; it crosses the inner zone of the belt (Boccaletti et al., 1977; Bemporad et al., 1986; Liotta, 1991) and played a role in controlling the Neogene geological evolution of the southern Tuscany and the Northern Tyrrhenian Sea (Ghelardoni, 1965; Bortolotti, 1966; Pascucci et al., 1999, 2007; Dini et al., 2008; Liotta et al., 2015; Rosenbaum and Piana Agostinetti, 2015; Liotta and Brogi, 2020). Inland, the Grosseto-Pienza tectonic lineament consists of a continuous morpho-structural lineament (at least 100 km long) delimiting, to the north, the Monte Amiata Geothermal area, and crossing the Siena-Radicofani Basin (Fig. 2) giving rise to the "Pienza threshold" that delimits the deeper (southern) basin, referred to as Radicofani Basin, with respect to the shallower (northern) one, named as Siena Basin (Liotta and Salvatorini, 1994; Liotta, 1996; Pascucci et al., 2007).

Few data are available on the setting of structures that define such a transfer zone. Some minor structures forming the Grosseto-Pienza tectonic lineament have been described in the Monte Leoni and Paganico areas (Fig. 2), where NE-trending faults characterised by strike-slip to

**Table 3**
Uranium isotopic composition and U-Th ages for the travertine deposits.

| Sample | $^{238}U$ | | $[^{234}U/^{238}U]$ | | $[^{230}Th/^{238}U]$ | | $[^{230}Th/^{232}Th]$ | | Age (ka) | | $[^{234}U/^{238}U]_{initial}$ | |
|---|---|---|---|---|---|---|---|---|---|---|---|---|
| ID | ppb | | activity | | activity | | activity | | corrected | | corrected | |
| BV2 * | 8.0 | ± 0.5 | 2.829 | ± 0.209 | 0.238 | ± 0.031 | 56.53 | ± 12.39 | 9.5 | ± 1.3 | 2.879 | ± 0.21 |
| BV3 * | 9.4 | ± 0.9 | 1.585 | ± 0.182 | 0.366 | ± 0.041 | 3.32 | ± 0.56 | 22.1 | ± 5.2 | 1.634 | ± 0.20 |
| BV4 * | 8.5 | ± 0.5 | 2.691 | ± 0.175 | 0.326 | ± 0.035 | 4.47 | ± 0.96 | 11.5 | ± 2.9 | 2.759 | ± 0.18 |
| BV6 * | 7.9 | ± 0.6 | 1.779 | ± 0.179 | 0.726 | ± 0.066 | 3.68 | ± 0.47 | 45.7 | ± 7.4 | 1.910 | ± 0.21 |
| BV10 ** | 18.768 | ± 0.056 [a] | 2.293 | ± 0.020 [a] | 0.2755 | ± 0.0057 | 8.2 | ± 0.4 | 12.6 | ± 0.7 | 2.340 | ± 0.021 |
| BV11 ** | 19.614 | ± 0.052 [a] | 2.271 | ± 0.026 [a] | 0.414 | ± 0.017 | 2.99 | ± 0.12 | 16.6 | ± 2.7 | 2.333 | ± 0.032 |
| BV12 ** | 26.421 | ± 0.038 [a] | 2.264 | ± 0.010 [a] | 0.699 | ± 0.050 | 0.935 | ± 0.070 | 9.5 | ± 1.8 | 2.30 | ± 0.11 |
| BV13 ** | 9.521 | ± 0.020 [a] | 1.987 | ± 0.012 [a] | 1.713 | ± 0.031 | 9.33 | ± 0.17 | 160.6 | ± 6.6 | 2.553 | ± 0.051 |
| BV15 ** | 21.394 | ± 0.036 [a] | 2.439 | ± 0.010 [a] | 0.3151 | ± 0.0047 | 16.79 | ± 0.29 | 14.3 | ± 0.4 | 2.498 | ± 0.011 |
| BV16 ** | 13.049 | ± 0.023 [a] | 2.344 | ± 0.014 [a] | 0.4752 | ± 0.0064 | 18.41 | ± 0.28 | 23.3 | ± 0.6 | 2.436 | ± 0.015 |

* α-counting; ** MC-ICPMS, chemistry was performed on December 28th, 2013 (Shen et al., 2003), and instrumental analysis on MC-ICP-MS (Shen et al., 2012). Analytical errors are 2σ of the mean. Decay constants used to calculate activity ratios are available in Cheng et al., 2013.
a$[^{238}U] = [^{235}U]$ x 137.818 (±0.65‰) (Hiess et al., 2019).

oblique-slip movements have been documented (Aldinucci et al., 2008; Brogi and Fulignati, 2012). Additional data are from Pienza area within the Radicofani Basin (Piccardi et al., 2017). The study area, located along the Grosseto-Pienza tectonic lineament, intersects the western shoulder of the Pliocene Basin, where it divided in its northern (Siena) and southern (Radicofani) part (Fig. 2).

Coexistence of NE-trending, left-lateral strike- to oblique-slip faults, and NW-trending normal faults has been documented in the outcrops of the basin substratum (Fig. 3). Nevertheless, the Siena and Radicofani basin ended its development during the middle Pliocene (Liotta, 1996; Pascucci et al., 2007; Brogi, 2011), suggesting that the NW-trending faults bounding the basin were no-more active during Quaternary. Conversely, we have documented the Pleistocene-Holocene age for the local NE-trending faults, implying their later/younger activity. These structures have been active even after the development of the Pliocene Basin. This can be once again explained considering the NE-trending structures as belonging to the regional transfer zone, now accommodating extension in the easternmost sector of the chain (Fig. 1). In this scenario, we do not exclude that some NW-trending fault segments, nearby or within the NE-trending shear zone, were reactivated during Quaternary, as it was the case during the travertine deposition and fissure ridges development (Fig. 3).

This tectonic scenario agrees to (i) the structural setting documented for the Monte Amiata area (Fig. 2), where Pleistocene-Holocene NE-trending faults influenced the volcanic centres localization and still control the geothermal fluids circulation (Brogi and Fabbrini, 2009), and (ii) to the tectonic framework defined for the Sarteano area (Fig. 2) where Quaternary NE-trending faults partially reactivated the Pliocene faults (Brogi et al., 2012).

Concerning the seismotectonics, our observations allow to confirm that the Grosseto-Pienza tectonic lineament is affected by recent-Present deformation, at least in the study sector. This is not in contrast with the observation by Piccardi et al. (2017) who highlighted active/capable faults in the surroundings of the study area. On the other hand, low-magnitude seismicity (M < 4) is recorded along the whole Grosseto-Pienza tectonic lineament, (http://cnt.rm.ingv.it) and in particular in the study area, where seismic events occurred in March 2018 nearby Bagno Vignoni (at least 22 events, M < 3). In this view, our data add useful information to better constrain the palaeoseismicity and neotectonic activity, as well as the seismotectonic context of this part of southern Tuscany.

## 6. Conclusions

Widespread long-lived (since 160 ka, at least) hydrothermal fluid circulation and travertine deposition took place along the wide (at least 3 km) Grosseto-Pienza NE-trending tectonic lineament, active during the development of the Neogene-Quaternary extension affecting the inner Northern Apennines. The palaeo-temperature and the isotopic composition of the hydrothermal fluids are similar to those of present-day thermal springs, accounting for a common tectonic scenario through time. This transfer zone is still active and able to produce low-magnitude (M < 4) seismicity (Fig. 15); such a setting has an important fallout for the seismic hazard assessment of southern Tuscany.

Travertine deposits formed from thermal springs aligned along transfer zone-fault segments and at their intersections with NW-trending faults. Faults permeability was guaranteed by the enhanced damaging at the intersection with the still active NE-trending faults that reopened the sealed fractures gaining a renewed permeability. The study of the travertine deposits, in terms of their architectural setting, facies distribution, ages and isotopic composition was essential for reconstructing the activity of faults, their permeability evolution and palaeo-fluids features. In this view, banded calcite veins offered the best opportunity to reconstruct the interplay between faulting, permeability evolution and fluids-flow in all geothermal areas characterised by bicarbonate-rich geothermal fluids. This picture underlines the role of the travertine deposits in reconstructing the neotectonic settings in geothermal areas.

## Author's contribution and authorship conformation form

All authors have participated in (a) conception and design, or analysis and interpretation of the data; (b) drafting the article or revising it critically for important intellectual content; and (c) approval of the final version.

## Acknowledgments

Support of the KH 125,584 project (NKFIH, National Research, Development and Innovation Office, Hungary), the TraRAS (Travertine Reservoir Analogue Studies) project, as well as the support of the European Union and the State of Hungary, co-financed by the European Regional Development Fund in the project of GINOP-2.3.2-15-2016-00009 'ICER' are gratefully acknowledged by S.K. E.C. is pleased to acknowledge a P.O.R.-F.S.E. 2007-2013 (Regional Competitiveness and Employment) grant from the Tuscan Regional Administration. U-Th dating was supported by the Ministry of Science and Technology (MOST) (107-2119-M-002-051 to C.-C.S.), the National Taiwan University (105R7625 to C.-C.S.), the Higher Education Sprout Project of the Ministry of Education, Taiwan ROC (107L901001 to C.-C.S.). We also acknowledge U.S. National Science Foundation grant EAR-1156134 to K.W.H. Comments and suggestions by Cihat Alçiçek and

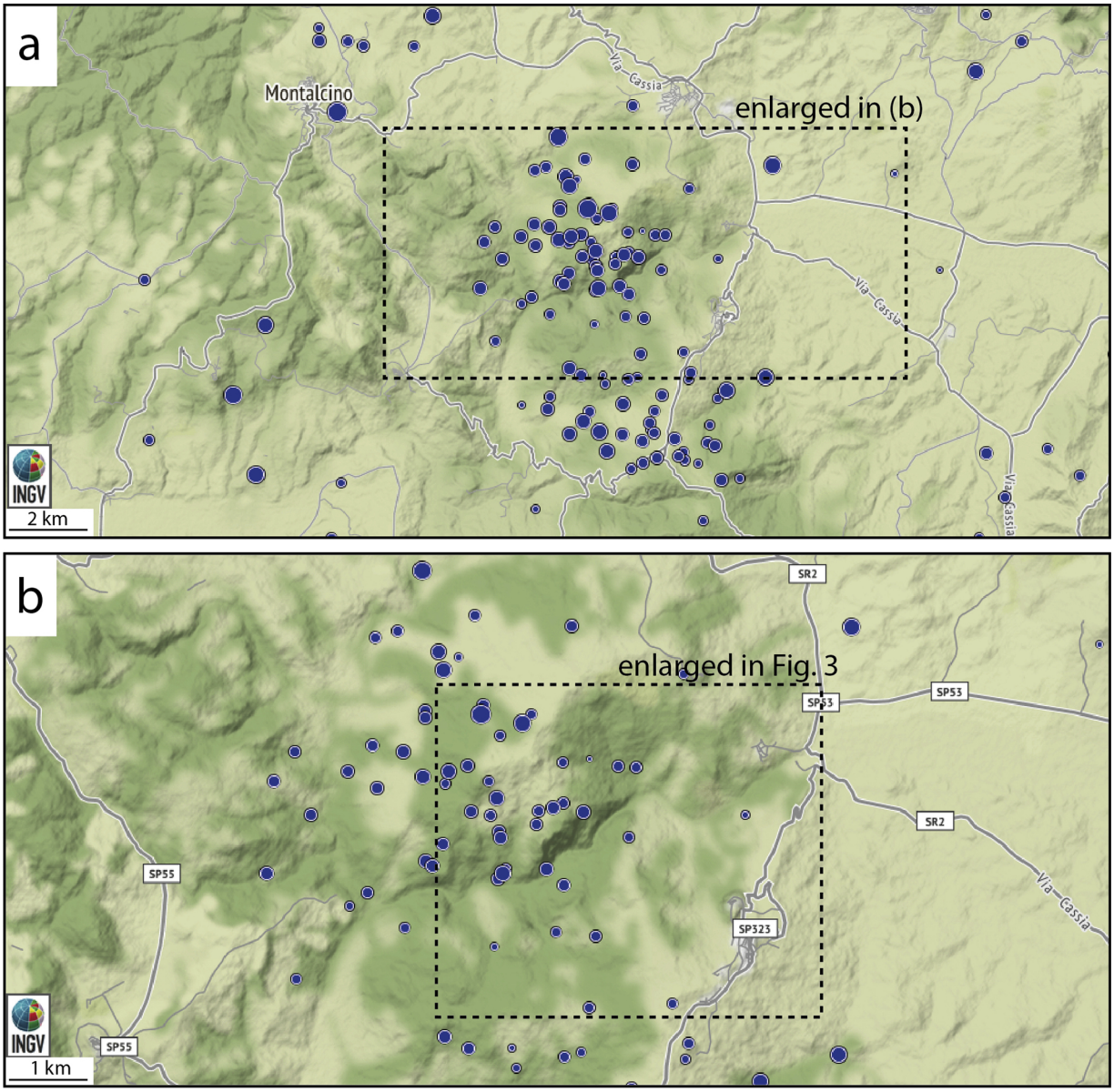


**Fig. 15.** Epicentres distribution (M < 4) in the study area and surroundings; diameter of circles indicate the earthquake magnitude ranging from 3,6 to 1; data record: 1985, January 1st – 2019 September 24nd (data from INGV: http://terremoti.ingv.it).

Eva Schill helped us to improve the original version of the manuscript.

## References


Acocella, V., Funiciello, R., 1999. The interaction between regional and local tectonics during resurgent doming: the case of the island of Ischia. Italy. J. Volcanol. Geotherm. Res. 88, 109–123.

Acocella, V., Funiciello, R., 2002. Transverse structures and volcanic activity along the Tyrrhenian margin of central Italy. Boll.Soc.Geol.Ital. 1, 739–747.

Acocella, V., Funiciello, R., 2006. Transverse systems along the extensional Tyrrhenian margin of central Italy and their influence on volcanism. Tectonics 25. https://doi.org/10.1029/2005TC001845.

Albarello, D., Batini, F., Bianciardi, P., Ciulli, B., Spinelli, E., Viti, M., 2005. Stress field assessment from ill-defined fault plane solutions: an example from the Larderello Geothermal Field (western Tuscany, Italy). Boll. Soc. Geol. It 3, 187–193.

Alçiçek, H., Bülbül, A., Yavuzer, İ., Alçiçek, M.C., 2019EEa. Hydrogeochemical and isotopic assessment and geothermometry applications of the Karahayıt Geothermal Field (Denizli Basin, SW Anatolia, Turkey). Hydrogeol. J.https://doi.org/10.1007/s10040-019-01927-y.

Alçiçek, H., Bülbül, A., Yavuzer, İ., Alçiçek, M.C., 2019EEb. Origin and evolution of the thermal waters from the Pamukkale Geothermal Field (Denizli Basin, SW Anatolia, Turkey): insights from hydrogeochemistry and geothermometry. J. Volcanol. Geotherm. Res. 372, 48–70.

Alçiçek, H., Bülbül, A., Capezzuoli, E., Brogi, A., Liotta, D., Meccheri, M., Ruggieri, G., Yavuzer, İ., Alçiçek, M.C., 2018. Origin, evolution and geothermometry of thermal waters in the Gölemezli Geothermal Field, Denizli Basin (SW Turkey). J. Volcanol. Geotherm. Res. 349, 1–30.

Alçiçek, H., Bülbül, A., Alçiçek, M.C., 2016. Hydrogeochemistry of the thermal waters from the Yenice Geothermal Field (Denizli Basin, SW Turkey). J. Volcanol. Geotherm. Res. 309, 118–138.

Alçiçek, M.C., Brogi, A., Capezzuoli, E., Liotta, D., Meccheri, M., 2013. Superimposed basins formation during the Neogene–quaternary extensional tectonics in SW-Anatolia (Turkey): insights from the kinematics of the Dinar Fault Zone. Tectonophysics 608, 713–727.

Alçiçek, M.C., Alçiçek, H., Altunel, E., Arenas, C., Bons, P., Brogi, A., Capezzuoli, E., de Riese, T., Della Porta, G., Gandin, A., Guo, L., Jones, B., Karabacak, V., Kershaw, S., Liotta, D., Mindszenty, A., Pedley, M., Ronchi, P., Swennen, R., Temiz, U., 2017. Comment on "First records of syn-diagenetic non-tectonic folding in Quaternary thermogene travertines caused by hydrothermal incremental veining" by Billi et al. Tectonophysics 721, 491–500.

Aldinucci, M., Pandeli, E., Sandrelli, F., 2008. Tectono-sedimentary evolution of the late palaeozoic–Early mesozoic metasediments of the Monticiano-Roccastrada Ridge (southern Tuscany, Northern Apennines, Italy). Boll. Soc. Geol. It 127, 567–579.

Altunel, E., Hancock, P.L., 1993a. Active fissuring and faulting in quaternary travertines at pamukkale, Western Turkey. In: In: Stewart, I.S., Vita-Finzi, C., Owen, L.A. (Eds.), Neotectonics and Active Faulting: Zeitschrift Fuer Geomorphologie Supplement 94. pp. 285–302.

Altunel, E., Hancock, P.L., 1993b. Morphology and structural setting of Quaternary travertines at Pamukkale. Turkey. Geol. J. 28, 335–346.

Altunel, E., Karabacak, V., 2005. Determination of horizontal extension from fissure-ridge travertines: a case study from the Denizli Basin, southwestern Turkey. Geodin. Acta 18, 333–342.
Anderson, T.R., Fairley, J.P., 2008. Relating permeability to the structural setting of a fault-controlled hydrothermal system in southeast Oregon, USA. J. Geophys. Res. 113. https://doi.org/10.1029/2007JB004962.
Bally, A.W., 1981. Atlantic type margins, in Geology of passive continental margins: history, structure and sedimentologic record: AAPG. Education Course Notes Series 19, 1–48.
Barbier, E., 2002. Geothermal energy and current status: an overview. Renew Sus Energy Rev 6, 3–65.
Barchi, M.R., De Feyter, A.J., Magnani, M.B., Minelli, G., Pialli, G., Sotera, B.M., 1998. Extensional tectonics in the Northern Apennines (Italy): evidence from the Crop03 deep seismic reflection line. Mem. Soc. Geol. It. 52, 527–538.
Barchi, M.R., 2010. The Neogene–quaternary evolution of the Northern Apennines: crustal structure, style of deformation and seismicity. J. Virtual Explor. 36. https://doi.org/10.3809/jvirtex.2009.00220.
Bartole, R., 1995. The North-Tyrrhenian–northern Apennines post-collisional system: constraints for a geodynamic model. Terranova 1, 7–30.
Batini, F., Brogi, A., Lazzarotto, A., Liotta, D., Pandeli, E., 2003. Geological features of larderello–travale and Mt amiata geothermal areas (southern Tuscany Italy). Episodes 26, 239–244.
Bemporad, S., Conedera, C., Dainelli, P., Ercoli, A., Facibeni, P., 1986. Landsat imagery: a valuatable tool for regional and structural geology. Mem. Soc. Geol. Ital. 31, 287–298.
Berardi, G., Vignaroli, G., Billi, A., Rossetti, F., Soligo, M., Kele, S., Baykara, M.O., Bernasconi, S.M., Castorina, F., Tecce, F., Shen, C., 2016. Growth of a Pleistocene giant carbonate vein and nearby thermogene travertine deposits at Semproniano, southern Tuscany, Italy: estimate of CO2 leakage. Tectonophysics 690, 219–239.
Bianchi, V., Ghinassi, M., Aldinucci, M., Boaga, J., Brogi, A., Deiana, R., 2015. Tectonically driven deposition and landscape evolution within upland incised valleys: ambra Valley fill, Pliocene–pleistocene, Tuscany. Italy. Sedimentology 62, 897–927.
Boccaletti, M., Elter, P., Guazzone, G.J.P., 1971. Plate tectonic models for the development of the western Alps and Northern Apennines. Nature 234, 108–111.
Boccaletti, M., Fazzuoli, M., Loddo, M., Mongelli, F., 1977. Heat flow measurements onthe Northern Apennines arc. Tectonophysics 41, 101–112.
Bonini, M., Moratti, G., 1995. Evoluzione tettonica del bacino neogenico di Radicondoli-Volterra (Toscana meridionale). Boll. Soc. Geol. It. 114, 549–573.
Bonini, M., Sani, F., 2002. Extension and compression in the northern Apennines (Italy) hinterland: evidence from the late Miocene-Pliocene Siena-Radicofani Basin and relations with basement structures. Tectonics 22, 1–35.
Bonini, L., Di Bucci, D., Toscani, G., Seno, S., Valensise, G., 2014. On the complexity of surface ruptures during normal faulting earthquakes: excerpts from the 6 April 2009 L'Aquila (central Italy) earthquake (Mw 6.3). Solid Earth 5, 389–408.
Bortolotti, V., 1966. La tettonica trasversale dell'Appennino. I-La linea Livorno-Sillaro. Boll. Soc. Geol. It. 85, 529–540.
Bossio, A., Costantini, A., Lazzarotto, A., Liotta, D., Mazzanti, R., Mazzei, R., Salvatorini, G., Sandrelli, F., 1993. Rassegna delle conoscenze sulla stratigrafia del Neoautoctono Toscano. Mem. Soc. Geol. Ital. 49, 17–98.
Bottinga, Y., 1968. Calculation of fractionation factors for carbon and oxygenisotopic exchange in the system calcite–carbon dioxide–water. J. Phys. Chem. 72, 800–808.
Brand, W.A., Assonov, S.S., Coplen, T.B., 2010. Correction for the 17O interference in δ13C measurements when analyzing $CO^2$ with stable isotope mass spectrometry (IUPAC Technical Report). Pure Appl. Chem. 82, 1719–1733.
Brogi, A., 2004a. Miocene low-angle detachments and upper crust megaboudinage in the Monte Amiata geothermal area (Northern Apennines, Italy). Geodin. Acta 17 (6), 375–387.
Brogi, A., 2004b. Faults linkage, damage rocks and hydrothermal fluid circulation: tectonic interpretation of the Rapolano Terme travertines (southern Tuscany, Italy) in the context of the Northern Apennines Neogene-Quaternary extension. Eclogae Geol. Helv. 97, 307–320.
Brogi, A., 2006. Neogene extension in the Northern Apennines (Italy): insights from the southern part of the Mt Amiata geothermal area. Geodin. Acta 19, 33–50.
Brogi, A., 2008a. The structure of the Monte Amiata volcano-geothermal area (Northern Apennines, Italy): neogene–quaternary compression versus extension. Int. J. Earth Sci. 97, 677–703.
Brogi, A., 2008b. Kinematics and geometry of Miocene low-angle detachments and exhumation of the metamorphic units in the hinterland of the Northern Apennines (Italy). J. Struct. Geol. 30, 2–20.
Brogi, A., 2011. Bowl-shaped basin related to low-angle detachment during continental extension: the case of the controversial Neogene Siena Basin (central Italy, Northern Apennines). Tectonophysics 499, 54–76.
Brogi, A., Lazzarotto, A., Liotta, D., Ranalli, G., 2005a. Crustal structures in the geothermal areas of southern Tuscany (Italy): insights from the CROP18 deep seismic reflection lines. J. Vol. Geoth. Res. 148, 60–80.
Brogi, A., Lazzarotto, A., Liotta, D., 2005b. CROP 18 Working Group,Structural features of southern Tuscany and geological interpretation of the CROP 18 seismic reflection survey. Italy. Boll. Soc. Geol. It 3, 213–236.
Brogi, A., Cornamusini, G., Sandrelli, F., 2005c. Geological setting of the Bagno Vignoni area (Nothern side of the Mt. Amiata geothermal area, Italy): collisional structures recorded in Tuscan Nappe. Boll. Soc. Geol. It., Vol. Spec. 3, 89–101.
Brogi, A., Lazzarotto, A., Grassi, S., 2007. The Bagno Vignoni 1 borehole log (Northern Mt. Amiata geothermal area, Southern Tuscany). Rend. Soc. Geol. It. 5, 84–87.
Brogi, A., Liotta, D., 2008. Highly extended terrains, lateral segmentation of the substratum, and basin development: the Middle–late Miocene Radicondoli Basin (inner northern Apennines, Italy). Tectonics 27, TC5002.
Brogi, A., Capezzuoli, E., 2009. Travertine deposition and faulting: the fault-related travertine fissure-ridge at Terme di S.Giovanni, Rapolano Terme (Italy). Int. J. Earth Sci. 98, 931–948.
Brogi, A., Fabbrini, L., 2009. Extensional and strike-slip tectonics across the Monte Amiata–Monte Cetona transect (Northern Apennines, Italy) and seismotectonic implications. Tectonophysics 476, 195–209.
Brogi, A., Liotta, D., Meccheri, M., Fabbrini, L., 2010a. Transtensional shear zones controlling volcanic eruptions: the Middle Pleistocene Monte Amiata volcano (inner Northern Apennines, Italy). Terra Nova 22, 137–146.
Brogi, A., Capezzuoli, E., Aqué, R., Branca, M., Voltaggio, M., 2010b. Studying travertine for neotectonics investigations: middle–late Pleistocene syntectonic travertine deposition at Serre di Rapolano (Northern Apennines, Italy). Geol. Rundschau 99, 1383–1398.
Brogi, A., Giorgetti, G., 2010. The tectono-metamorphic record of the Tuscan Nappe from the Colline Metallifere region (Northern Apennines, Italy). Ital. J. Geosci. 129, 177–187.
Brogi, A., Fabbrini, L., Liotta, D., 2011. Sb–Hg ore deposit distribution controlled by brittle structures: the case of the Selvena mining district (Monte Amiata, Tuscany, Italy). Ore Geol. Rev. 41, 35–48.
Brogi, A., Fulignati, P., 2012. Tectonic control on hydrothermal circulation and fluid evolution in the Pietratonda–Poggio Peloso (southern Tuscany, Italy) carbonate-hosted Sb-mineralization. Ore Geol. Rev. 44, 158–171.
Brogi, A., Capezzuoli, E., Buracchi, E., Branca, M., 2012. Tectonic control on travertine and calcareous tufa deposition in a low-temperature geothermal system (Sarteano, Central Italy). Journal of the Geological Society, London 169, 461–476.
Brogi, A., Giorgetti, G., 2012. Tectono-metamorphic evolution of the siliciclastic units in the Middle Tuscan Range (inner Northern Apennines): Mg-carpholite bearing quartz veins related to syn-metamorphic syn-orogenic foliation. Tectonophysics 526-529, 167–184.
Brogi, A., Fidolini, F., Liotta, D., 2013. Tectonic and sedimentary evolution of the Upper Valdarno Basin: new insights from the lacustrine S. Barbara Basin. Italian Journal of Geoscience 132, 81–97.
Brogi, A., Capezzuoli, E., 2014. Earthquake impact on fissure-ridge type travertine deposition. Geol. Mag. 151, 1135–1143.
Brogi, A., Capezzuoli, E., Martini, I., Picozzi, M., Sandrelli, F., 2014. Late Quaternary tectonics in the inner Northern Apennines (Siena Basin, southern Tuscany, Italy) and their seismotectonic implication. J. Geodyn. 76, 25–45.
Brogi, A., Alçiçek, M.C., Yalçıner, C.C., Capezzuoli, E., Liotta, D., Meccheri, M., Rimondi, V., Ruggieri, G., Gandin, A., Boschi, C., Büyüksaraç, A., Alçiçek, H., Bülbül, A., Baykara, M.O., Shen, C.-C., 2016. Hydrothermal fluids circulation and travertine deposition in an active tectonic setting: insights from the Kamara geothermal area (western Anatolia, Turkey). Tectonophysics 680, 211–232.
Brogi, A., Capezzuoli, E., Kele, K., Baykara, M.O., Shen, C., 2017. Key travertine tectofacies for neotectonics and palaeoseismicity reconstruction: effects of hydrothermal overpressured fluid injection. J. Geol. Soc. 174 (4), 679.
Brogi, A., Capezzuoli, E., Moretti, M., Olvera-García, E., Matera, P.F., Garduno-Monroy, V., Mancini, A., 2018. Earthquake-triggered soft-sediment deformation structures (seismites) in travertine deposits. Tectonophysics 745, 349–365.
Brunet, C., Monié, P., Jolivet, L., Cadet, J.P., 2000. Migration of compression and extension in the Tyrrhenian Sea, insights from $^{40}Ar/^{39}Ar$ ages on micas along a transect from Corsica to Tuscany. Tectonophysics 321, 127–155.
Buonasorte, G., Fiordelisi, A., Rossi, U., 1987. Tectonic structures and geometric setting of the Vulsini Volcanic Complex. Periodico di Mineralogia 56, 123–136.
Burgener, L., Huntington, K.W., Hoke, G.D., Schauer, A., Ringham, M.C., Latorre, C., Díaz, F.P., 2016. Variations in soil carbonate formation and seasonal bias over &4 km of relief in the western Andes (30°S) revealed by clumped isotope thermometry. Earth Planet. Sci. Lett. 441, 188–199.
Çakır, Z., 1999. Along-strike discontinuity of active normal faults and its influence on quaternary travertine deposition: examples from western Turkey. Turk. J. Earth Sci. 8, 67–80.
Caine, S.J., Evans, J.P., Forster, C.B., 1996. Fault zone architecture and permeability structure. Geology 24, 1025–1028.
Calamai, A., Cataldi, R., Squarci, P., Taffi, L., 1970. Geology geophysics and hydrogeology of the Monte Amiata geothermal field. Geothermics 1, 1–9.
Calcagnile, G., Panza, G., 1981. The main characteristics of the lithosphere asthenosphere system in Italy and surrounding regions. Pure Appl. Geophys. 119, 865–879.
Capezzuoli, E., Gandin, A., Pedley, H.M., 2014. Decoding tufa and travertine (freshwater carbonates) in the sedimentary record: the state of the art. Sedimentology 61, 1–21.
Capezzuoli, E., Ruggieri, G., Rimondi, V., Brogi, A., Liotta, D., Alçiçek, M.C., Alçiçek, H., Bülbül, A., Gandin, A., Meccheri, M., Shen, C.-C., Baykara, M.O., 2018. Calcite veining and feeding conduits in a hydrothermal system: insights from a natural section across the Pleistocene Gölemezli travertine depositional system (western Anatolia, Turkey). Sediment. Geol. 364, 180–203.
Carmignani, L., Kligfield, R., 1990. Crustal extension in the Northern Apennines: transition from compression to extension in the Alpi Apuane core complex. Tectonics 9, 1275–1303.
Carmignani, L., Decandia, F.A., Disperati, L., Fantozzi, P.L., Lazzarotto, A., Liotta, D., Meccheri, M., 1994. Tertiary extensional tectonics in Tuscany (Northern Apennines Italy). Tectonophysics 238, 295–315.
Carmignani, L., Decandia, F.A., Disperati, L., Fantozzi, P.L., Lazzarotto, A., Liotta, D., Oggiano, G., 1995. Relationships between the Sardinia–Corsica–Provencal domain and the Northern Apennines. Terra Nova 7, 128–137.
Carmignani, L., Decandia, F.A., Disperati, L., Fantozzi, P.L., Kligfield, R., Lazzarotto, A., Liotta, D., Meccheri, M., 2001. Inner Northern apennines. In: Vai, G.B., Martini, I.P. (Eds.), Anatomy of an Orogen: the Apennines and Adjacent Mediterranean Basins. Kluwer, Dordrecht.

Cadoux, A., Pinti, D.L., 2009. Hybrid character and pre-eruptive events of Mt Amiata volcano (Italy) inferred from geochronological, petro-geochemical and isotopic data. J. Volcanol. Geotherm. Res. 179, 169–190.
Cheng, H., Edwards, L.R., Shen, C.C., Polyak, V.J., Asmerom, Y., Woodhead, J., Hellstrom, J., Wang, Y., Kong, X., Spötl, C., Wang, X., Calvin, A.E., 2013. Improvements in 230Th dating, 230Th and 234U half-life values, and U–Th isotopic measurements by multi-collector inductively coupled plasma mass spectrometry. Earth Planet. Sci. Lett. 371, 82–91.
Claes, H., Erthal, M.M., Soete, J., Özkul, M., Swennen, R., 2017. Shrub and pore type classification: petrography of travertine shrubs from the Ballık-Belevi area (Denizli, SW Turkey). Quat. Int. 437, 147–163.
Collettini, C., De Paola, N., Holdsworth, R.E., Barchi, M.R., 2006. The development and behaviour of low-angle normal faults during Cenozoic asymmetric extension in the Northern Apennines. Italy. J. Struct. Geol. 28, 333–352.
Coplen, T.B., 2007. Calibration of the calcite–water oxygenisotope geothermometer at Devils Hole, Nevada, a natural laboratory. Geochim. Cosmochim. Acta 71, 3948–3957.
Cox, S.F., Knackstedt, M.A., Braun, J., 2001. Principles of structural control on permeability and fluid flow in hydrothermal systems (Structural controls on ore genesis). Society of Economic Geologists 24, 1–24 Chapter 1.
Curewitz, D., Karson, J.A., 1997. Structural settings of hydrothermal outflow: fracture permeability maintained by fault propagation and interaction. J. Volcanol. Geotherm. Res. 79, 149–168.
Dallmeyer, R.D., Liotta, D., 1998. Extension, uplift of rocks and cooling ages in thinned crustal provinces: the Larderello geothermal area (inner northern Apennines, Italy). Geol. Mag. 135, 193–202.
Decandia, F.A., Lazzarotto, A., Liotta, D., 1993. La "'Serie ridotta"' nel quadro dell'evoluzione geologica della Toscana meridionale. Mem. Soc. Geol. It. 49, 181–190.
Dennis, K.J., Affek, H.P., Passey, B.H., Schrag, D.P., Eiler, J.M., 2011. Defining an absolute reference frame for 'clumped' isotope studies of CO2. Geochim. Cosmochim. Acta 75 (22), 7117–7131.
Di Bucci, D., Mazzoli, S., 2002. Active tectonics of the Northern Apennines and Adria geodynamics: new data and a discussion. J. Geodyn. 34, 687–707.
Di Stefano, R., Chiarabba, C., Chiaraluce, L., Cocco, M., De Gori, P., Piccinini, D., Valoroso, L., 2011. Fault zone properties affecting the rupture evolution of the 2009 (Mw6.1) L' Aquila earthquake (central Italy): insights from seismic tomography. Geophys. Res. Lett. 38, l10310. https://doi.org/10.1029/2011gl047365.
Dini, A., Mazzarini, F., Musumeci, G., Rocchi, S., 2008. Multiple hydro-fracturing by boron-rich fluids in the Late Miocene contact aureole of eastern Elba Island (Tuscany, Italy). Terra Nova 20, 318–326.
Doglioni, C., 1991. A proposal of kinematic modeling forW-dipping subductions. Possible applications to the Tyrrhenian-Apennines system. Terra Nova 3 (423), 434.
Ebinger, C.J., 1989. Geometric and kinematic development of border faults and accommodation zones, Kivu-Rusizi rift. Africa. Tectonics 8, 117–137.
Edwards, R.L., Chen, J.H., Wasserburg, G.J., 1988. $^{238}$U–$^{234}$U–$^{230}$Th systematics and the precise measurement of time over the last 500,000 years. Earth Planet. Sci. Lett. 81, 175–192.
Erthal, M.M., Capezzuoli, E., Mancini, A., Claes, H., Soete, J., Swennen, R., 2017. Shrub morpho-types as indicator for the water flow energy - Tivoli travertine case (Central Italy). Sediment. Geol. 347, 79–99.
Faccenna, C., Soligo, M., Billi, A., De Filippis, L., Funiciello, R., Rossetti, C., Tuccimei, P., 2008. Late Pleistocene depositional cycles of the Lapis Tiburtinus travertine (Tivoli, Central Italy): possible influence of climate and fault activity. Glob. Planet. Chang. 63, 299–308.
Ferrari, L., Conticelli, S., Burlamacchi, L., Manetti, P., 1996. Volcanological evolution of the Monte Amiata, Southern Tuscany: new geological and petrochemical data. Acta Vulcanologica 8, 41–56.
Finetti, I.R., Boccaletti, M., Bonini, M., Del Ben, A., Geletti, R., Pipan, M., Sani, F., 2001. Crustal section based on CROP seismic data across the North Tyrrhenian-Northern Apennines-Adriatic Sea. Tectonophysics 343, 135–163.
Finetti, I.R., 2006. Basic regional crustal setting and superimposed local plutonintrusion related tectonics in the Larderello-Monte Amiata geothermal province, from integrated CROP seismic data. Boll. Soc. Geol. It 125, 117–146.
Gandin, A., Capezzuoli, E., 2014. Travertine: distinctive depositional fabrics of carbonates from thermal spring systems. Sedimentology 61, 264–290.
Ghelardoni, G., 1965. Osservazioni sulla tettonica trasversale dell'Appennino settentrionale. Boll. Soc. Geol. It. 93, 837–860.
Gibbs, A.D., 1990. Linked fault families in basin formation. J. Struct. Geol. 12, 795–803.
Gualtieri, L., Bertotti, G., Cloetingh, S., 1998. Lateral variation of thermo-mechanical properties in the Tyrrhenian Northern Apennine region. Tectonophysics 300, 143–158.
Guo, L., Riding, R., 1999. Rapid facies changes in Holocene fissure ridge hot spring travertines, Rapolano Terme. Italy. Sedimentology 46, 1145–1158.
Hancock, P.L., Chalmers, R.M.L., Altunel, E., Çakır, Z., 1999. Travitonics: using travertines in active fault studies. J. Struct. Geol. 21, 903–916.
He, B., Olack, G.A., Colman, A.S., 2012. Pressure baseline correction and high-precision CO2 clumped isotope (Δ47) measurements in bellows and micro-volume modes. Rapid Commun. Mass Spectrom. 26, 2837–2853.
Henchiri, M., Ahmed, W.B., Brogi, A., Alçiçek, M.C., Benassi, R., 2017. Evolution of Pleistocene travertine depositional system from terraced slope tofissure-ridge in a mixed travertine-alluvial succession (Jebel El Mida, Gafsa, southern Tunisia). Geodin. Acta 29, 20–41.
Hiess, J.Condon, D.J., McLean, N., Noble, S.R., 212. U-238/U-235 Systematics in Terrestrial Uranium-Bearing Minerals. Science 335, 1610-1618.
Hoefs, J., 1997. Stable Isotope Geochemistry. Springer-Verlag, Berlin 201 p.
Jolivet, L., Dubois, R., Fournier, R., Goffe', B., Michard, A., Jourdan, C., 1990. Ductile extension in alpine Corsica. Geology 18, 1007–1010.
Karabacak, V., Uysal, I.T., Mutlu, H., Ünal-İmer, E., Dirik, R.K., Feng, Y., Akıska, S., Aydoğdu, İ., Zhao, J., 2019. Are U-Th dates correlated with historical records of earthquakes? Constraints from co-seismic carbonate veins within the North Anatolian Fault Zone. Tectonicshttps://doi.org/10.31223/osf.io/kbt6p.
Kele, S., Breitenbach, S.F.M., Capezzuoli, E., Meckler, A.N., Ziegler, M., Millan, I.M., Kluge, T., Deák, J., Hanselmann, K., John, C.M., Yan, H., Liu, Z., Bernasconi, S.M., 2015. Temperature dependence of oxygen- and clumped isotope fractionation in carbonates: a study of travertines and tufas in the 6–95 _C temperature range. Geochimica et Cosmichimica Acta 168, 172–192.
Kele, S., Özkul, M., Fórizs, I., Gökgöz, A., Baykara, M.O., Alçiçek, M.C., Németh, T., 2011. Stable isotope geochemical study of Pamukkale travertines: new evidences of low-temperature non-equilibrium calcite-water fractionation. Sediment. Geol. 238, 191–212.
Kelson, J.R., Huntington, K.W., Schauer, A.J., Saenger, C., Lechler, A.R., 2017. Toward a universal carbonate clumped isotope calibration: diverse synthesis and preparatory methods suggest a single temperature relationshi Geochim. Cosmochim. Acta 197, 104–131.
Kim, S.-T., O'Neil, J.R., 1997. Equilibrium and nonequilibrium oxygen isotope effects in synthetic carbonates. Geochim. Cosmochim. Acta 61, 3461–3475.
Kim, Y.-S., Peacock, D.C.P., Sanderson, D.J., 2003. Strike-slip faults and damage zones at Marsalforn, Gozo Island. Malta. J. Struct. Geol. 25, 793–812.
Lavecchia, G., 1988. The Tyrrhenian-Apennines system: structural setting and seismotectogenesis. Tectonophysics 147, 263–296.
Lavecchia, G., Boncio, P., Creati, N., Brozzetti, F., 2004. Stile strutturale stato termomeccanico e significato sismogenetico del thrust adriatico: dati e spunti da una revisione del profilo CROP 03 integrata con l'analisi di dati sismologici. Boll. Soc. Geol. It. 123, 111–126.
Lazzarotto, A., Mazzanti, R., 1978. Geologia dell'alta Val Di Cecina. Boll. Soc. Geol. It. 95, 1365–1487.
Liotta, D., 1991. The arbia-val marecchia line, Northern Apennines. Eclogae Geolicae Helvetiae 84 (2), 413–430.
Liotta, D., 1994. Structural features of the Radicofani basin along the Piancastagnaio (Monte Amiata)–S.CAsciano dei Bagni (Monte Cetona) cross section. Mem. Soc. Geol. It. 48, 401–408.
Liotta, D., 1996. Analisi del settore centro-meridionale del Bacino pliocenico di Radicofani, Toscana meridionale. Boll. Soc. Geol. Ital. 115, 115–143.
Liotta, D., Salvatorini, G., 1994. Evoluzione sedimentaria e tettonica della parte centromeridionale del bacino pliocenico di Radicofani. Studi Geol. Camerti Spec. 1, 65–77.
Liotta, D., Ranalli, G., 1999. Correlation between seismic reflectivity and rheology in extended lithosphere: southern Tuscany inner Northern Apennines Italy. Tectonophysics 315, 109–122.
Liotta, D., Cernobori, L., Nicolich, R., 1998. Restricted rifting and its coexistence with compressional structures: results from the Crop03 traverse (Northern Apennines Italy). Terra Nova 10, 16–20.
Liotta, D., Brogi, A., Meccheri, M., Dini, A., Bianco, C., Ruggieri, G., 2015. Coexistence of low-angle normal and high-angle strike- to oblique-slip faults during Late Miocene mineralization in eastern Elba Island (Italy). Tectonophysics 660, 17–34.
Locardi, E., Nicolich, R., 1992. Geodinamica del Tirreno e dell'Appennino centro-meridionale: la nuova carta della Moho. Mem. Soc. Geol. Ital. 41, 121–140.
Losacco, U., 1959. Ricerche geologiche nella Toscana meridionale II. Affioramenti mesozoici della media Val d'Orcia: bagno Vignoni, Rocca d'Orcia, Ripa d'Orcia e Pienza (Siena). Boll. Soc. Geol. It. 78, 101–120.
Liotta, D., Brogi, A., 2020. Pliocene-Quaternary fault kinematics in the Larderello geothermal area (Italy): insights for the interpretation of the present stress field. Geothermics 83, 101714. https://doi.org/10.1016/j.geothermics.2019.101714.
Lister, G.S., Etheridge, M.A., Symonds, P.A., 1986. Detachment faulting and the evolution of passive continental margins. Geology 14, 246–250.
Ludwig, K.R., 2003. Isoplot/Ex Version 3.00, a Geochronological Toolkit for Microsoft Excel. Berkeley Geochronology Center. Special Publication p. 4.
Mantovani, E., Albarello, D., Tamburelli, C., Babbucci, D., 1995. Evolution of the Tyrrhenian basin and surrounding regions as a result of the Africa-Eurasia convergence. J. Geod. 21, 35–72.
Mantovani, E., Viti, M., Babbucci, D., Tamburelli, C., Cenni, N., Baglione, M., D'Intinosante, V., 2015. Present Tectonic Setting and Spatio-Temporal Distribution of Seismicity in the Apennine Belt. Int. J. Geosci. 6, 429–454.
Martini, I.P., Sagri, M., 1993. Tecto-sedimentary characteristics and the genesis of the recent magmatism of Southern Tuscany and Northern Latium. Per. Mineral. 56, 157–172.
Mazzanti, R., 1966. Geologia della zona di Pomarance-Larderello (Prov. Di Pisa). Mem. Soc. Geol. Ital. 5, 105–138.
Mazzuoli, R., Tortorici, L., Ventura, G., 1995. Oblique rifting in Salina, lipari and Vulcano islands (Aeolian islands, southern Italy). Terra Nova 7, 444–452.
Mesci, B.L., Gursoy, H., Tatar, O., 2008. The evolution of travertine masses in the Sivas Area (Central Turkey) and their relationships to active tectonics. Turk. J. Earth Sci. 17, 219–240.
Micklethwaite, S., Cox, S.F., 2004. Fault-segment rupture, aftershock-zone fluid flow, and mineralization. GSA Geology 32, 813–816.
Minissale, A., 2004. Origin, transport and discharge of $CO^2$ in central Italy. Earth. Rev. 66 (1–2), 89–141.
Molli, G., 2008. Northern Apennine–corsica orogenic system: an updated overview. Geol. Soc. Lond. Spec. Publ. 298, 413–442.
Muir-Wood, R., 1993. Neohydrotectonics. Zschr Geomorph Suppl 94, 275–284.
Negredo, A.M., Barba, S., Carminati, E., Sabadini, R., Giunchi, C., 1999. Contribution of numeric dynamic modelling to the understanding of the seismotectonic regime of the

Northern Apennines. Tectonophysics 315, 15–30.
Pandeli, E., Bertini, G., Castellucci, P., 1991. The tectonic wedges complex of the Larderello area (Southern Tuscany, Italy). Boll. Soc. Geol. It. 110, 621–629.
Panichi, C., Tongiorgi, E., 1976. Carbon isotopic composition of CO2 from springs, fumaroles,mofettes and travertines of central and southern Italy: a preliminary prospection method of geothermal area. In: Proc. 2nd UN Symposium on the Development and Use of Geothermal Energy. San Francisco. U.S.A., Pp. 815–825 Pentecost, A., 2005. Travertine, Geologist Association. Springer-Verlag, Berlin. 445.
Pascucci, V., Merlini, S., Martini, I.P., 1999. Seismic stratigraphy of the Miocene-Pleistocene sedimentary basins of the Northern Tyrrhenian Sea and western Tuscany (Italy). Basin Res. 11, 337–356.
Pascucci, V., Costantini, A., Martini, I.P., Dringoli, R., 2006. Tectono-sedimentary analysis of a complex, extensional, Neogene basin formed on thrust-faulted, Northern Apennines hinterland: radicofani Basin. Italy. Sed. Geol. 183, 81–97.
Pascucci, V., Martini, I.P., Sagri, M., Sandrelli, F., 2007. Effects of transverse structural lineaments on the Neogene–quaternary basins of tuscany (inner Northern apennines, Italy). In: In: Nichols, G., Williams, E., Paola, C. (Eds.), Sedimentary Processes, Environments and Basins: a Tribute to Peter Friend. Intern. Ass. Sediment., Spec. Publ. 38. pp. 155–182.
Patacca, E., Sartori, R., Scandone, P., 1990. Tyrrhenian basin and Apenninic arcs: kinematic relations since Late Tortonian times. Mem. Soc. Geol. Ital. 45, 425–451.
Pentecost, A., 1994. Formation of laminate travertines at Bagno Vignone. Italy. Geomicrobiology 12, 239–251.
Pentecost, A., 2005. Travertine. Springer, Berlin 445 pp.
Piccardi, L., Vittori, E., Blumetti, A.M., Quaternary, V.C., 2017. Mapping capable faulting hazard in a moderate-seismicity, high heat-flow environment: the Tuscia province (southern Tuscany-northern Latium, Italy). Quat. Int. 451, 11–36.
Rimondi, V., Costagliola, P., Ruggieri, G., Benvenuti, M., Boschi, C., Brogi, A., Capezzuoli, E., Morelli, G., Gasparon, M., Liotta, D., 2015. Investigating fossil hydrothermal systems by means of fluid inclusions and stable isotopes in banded travertine: an example from Castelnuovo dell'Abate (southern Tuscany, Italy). Int. J. Earth Sci. 105 (22), 659–679.
Ronchi, P., Cruciani, F., 2015. Continental carbonates as a hydrocarbon reservoir, an analog case study from the travertine of Saturnia. Italy. AAPG Bulletin 99, 711–734.
Rosenbaum, G., Piana Agostinetti, N., 2015. Crustal and upper mantle responses to lithospheric segmentation in the northern Apennines. Tectonics 34, 648–661.
Rossetti, F., Faccenna, C., Jolivet, L., Funiciello, R., Tecce, F., Brunet, C., 1999. Syn-versus post-orogenic extension: the case study of Giglio Island (Northern Tyrrenian Sea, Italy). Tectonophysics 304, 73–92.
Rossetti, F., Faccenna, G., Jolivet, L., Goffé, B., Funiciello, R., 2002. Structural signature and exhumation P–T–t paths of the blueschist units exposed in the interior of the Northern Apennine chain, tectonic implications. Boll. Soc. Geol. It, Spec. Vol. 1, 829–842.
Rossetti, F., Glodny, J., Theye, T., Maggi, M., 2015. Pressure–temperature–deformation–time of the ductile Alpine shearing in Corsica: fromorogenic construction to collapse. Lithos 218–219, 99–116.
Rowland, J.V., Sibson, R.H., 2004. Structural controls on hydrothermal flowin a segmented rift system, Taupo Volcanic Zone, New Zealand. Geofluids 4, 259–283.
Schauer, A.J., Kelson, J., Saenger, C., Huntington, K.W., 2016. Choice of 17O correction affects clumped isotope (Δ47) values of CO2 measured with mass spectrometry. Rapid Commun. Mass Spectrom. 30, 2607–2616.
Serri, G., Innocenti, F., Manetti, P., 1993. Geochemical and petrological evidence of the subduction of delaminated Adriatic continental lithosphere in the genesis of the Neogene-Quaternary magmatism of Central Italy. Tectonophysics 223, 117–147.
Shen, C.-C., Cheng, H., Edwards, R.L., Moran, S.B., Edmonds, H.N., Hoff, J.A., Thomas, R.B., 2003. Measurement of attogram quantities of 231Pa in dissolved and particulate fractions of seawater by isotope dilution thermal ionization mass spectroscopy. Anal. Chem. 75, 1075–1079.
Shen, C.-C., Wu, C.-C., Cheng, H., Edwards, R.L., Hsieh, Y.-T., Gallet, S., Chang, C.-C., Li, T.-Y., Lam, D.D., Kano, A., Hori, M., Spötl, C., 2012. High-precision and high resolution carbonate 230Th dating by MC-ICP-MS with SEM protocols. Geochim. Cosmochim. Acta 99, 71–86.
Sibson, R.H., 1987. Earthquake rupturing as a mineralising agent in hydrothermal systems. Geology 15, 704–710.
Signorini, R., 1935. Linee tettoniche trasversali nell'Appennino settentrionale. Rend. R. Accad. Naz. Lincei 21, 42–45.
Spötl, C., Vennemann, T.W., 2003. Continuous-flow IRMS analysis of carbonate minerals. Rapid Commun. Mass Spectrom. 17, 1004–1006.
Storti, F., 1995. Tectonics of the Punta Bianca promontory: insights for the evolution of the northern Apennines-northern Tyrrheman Sea basin. Tectonics 14, 832–847.
Temiz, U., Gokten, E., Eikenberg, J., 2009. U/Th dating of fissure ridge travertines from the Kirsehir region (central Anatolia, Turkey); structural relations and implications for the neotectonic development of the Anatolian block. Geodin. Acta 22, 201–213.
Temiz, U., Eikenberg, J., 2011. U/Th dating of the travertine deposited at transfer zone between two normal faults and their neotectonic significance: cambazli ridge travertines (the Gediz graben, Turkey). Geodin. Acta 24, 95–105.
Temiz, U., Gökten, Y.E., Eikenberg, J., 2013. Strike-slip deformation and U/Th dating of travertine deposition: examples from North Anatolian Fault Zone, Bolu and yeniçağ basins. Turkey. Quaternary International 312, 132–140.
Török, A., Claes, H., Brogi, A., Liotta, D., Tóth, A., Mindszenty, A., Kudó, I., Kele, S., Huntington, K.W., Shen, C., Swennen, R., 2019. A multi–methodological approach to reconstruct the configuration of a travertine fissure ridge system: the case of the Cukor quarry (Süttő, Gerecse Hills, Hungary). Geomorphology 345, 106836. https://doi.org/10.1016/j.geomorph.2019.106836.
Uysal, I.T., Feng, Y., Zhao, J.X., Altunel, E., Weatherley, D., Karabacak, V., Cengiz, O., Golding, S.D., Lawrence, M.G., Collerson, K.D., 2007. U-series dating and geochemical tracing of late Quaternary travertine in co-seismic fissures. Earth Planet. Sci. Lett. 257 (3–4), 450–462.
Uysal, I.T., Feng, Y., Zhao, J.X., Isik, V., Nuriel, P., Golding, S.D., 2009. Hydrothermal CO2 degassing in seismically active zones during the late Quaternary. Chem. Geol. 265, 442–454.
Vai, G.B., Martini, I.P., 2001. Anatomy of an Orogen: The Apennines and Adjacent Mediterranean Basins. Kluwer Academic Publishers p. 631.
Vignaroli, G., Berardi, G., Billi, A., Kele, S., Rossetti, F., Soligo, M., Bernasconi, S.M., 2016. Tectonics, hydrothermalism, and paleoclimaterecorded by Quaternary travertines and their spatio-temporal distribution in the Albegna basin, central Italy: insights on Tyrrhenian margin neotectonics. Lithosphere 8, 335–358.
Viti, M., Mantovani, E., Babbucci, D., Tamburelli, C., 2006. Quaternary Geodynamics and deformation pattern in the southern apennines: implications for seismic activity Boll. Soc. Geol. It 125, 273–291.
Wedepohl, K., 1995. The composition of the continental crust. Geochim. Cosmochim. Acta 59, 1217–1239.
Williams, R.T., Goodwin, L.B., Sharp, W.D., Mozley, P.S., 2017. Reading a 400,000-year record of earthquake frequency for an intraplate fault. PNAS 114, 4893–4898.
Zucchi, M., Brogi, A., Liotta, D., Rimondi, V., Ruggieri, V., Montegrossi, G., Caggianelli, A., Dini, A., 2017. Permeability and hydraulic conductivity of faulted micaschist in the eastern Elba Island exhumed geothermal system (Tyrrhenian sea, Italy): insights from Cala Stagnone. Geothermics 70, 125–145.